Evolution of the structure with the composition and the defect arrangement in the gadolinium and samarium doped and co-doped ceria systems: A molecular dynamics study

Serge Vives, David Ramel, Cathy Meunier

Version of Record: https://www.sciencedirect.com/science/article/pii/S0167273821000643
Manuscript_e0599400ab0c92c18095650e10494dbf

Evolution of the structure with the composition and the defect arrangement in the gadolinium and samarium doped and co-doped ceria systems: A Molecular Dynamics study

Serge Vives [a,§], David Ramel[a], Cathy Meunier[b]

[a)] *FEMTO-ST Institute, Univ. Bourgogne Franche-Comte, CNRS, 2 avenue Jean Moulin 90000 Belfort, France.*
[b)] *Nanomedecine, Imagerie, Therapeutique, Univ. Bourgogne Franche-Comte, 4 place Tharradin, 25211 Montbéliard, France.*

§ corresponding author
serge.vives@univ-fcomte.fr

Abstract

We investigate the evolution of the fluorite structure in the $Ce_{1-x}M_xO_{2-x/2}$ system with Gd and Sm as Rare Earth (RE) doping cations and Gd/Sm as co-doping couple using Molecular Dynamics at 298 K. Doping cations and oxygen vacancies are introduced in the CeO_2 fluorite lattice through two different arrangements the Random one and the Neighbour one. The evolution of the lattice parameter is compared with different models and experimental data extracted from the literature. Results concerning the chemical expansion and the oxygen vacancy radius are commented. The calculation of the Radial Distribution Function (RDF) allows to observe two components for the Ce-Ce, Ce-M and M-M (M= Gd, Sm, Gd/Sm) bond length as it is the case in the C-type RE_2O_3 structure. The percolation concept is introduced and discussed based on the evolution of the M-M group size distribution and the M-O coordination number.

Keywords: Doped ceria, co-doped ceria, Molecular Dynamics, Structure, Percolation.

1. Introduction

In the last few years a lot of attention has been paid to CeO_2-based materials. This interest is in large part due to the high ionic conductivity at relatively moderate temperature (500°C - 700°C) of Rare Earth (RE) doped CeO_2 [1-3] essential for a future commercial application in Solid Oxide Fuel (and/or Electrolysis) Cell technology [4-6]. Such materials are also under investigation in other research fields as bio sensor [7], catalysis [8] or electrostriction [9].

Once CeO_2 doped with aliovalent cations, oxygen vacancies are created in order to maintain the charge neutrality of the structure. In the case of a RE^{3+} dopant the introduction of two foreign ions in the CeO_2 fluorite structure generates one oxygen vacancy following the relation (1):

$$RE_2O_3 \rightarrow 2RE'_{Ce} + 3O_O^x + V_O^{\bullet\bullet} \quad (1)$$

This vacancy will be more or less mobile according to its energetical environment. Indeed, to move from one site to another an oxygen vacancy has to overcome an energy barrier which is a function of the migration and the defect association enthalpies [1, 10].

The distribution of dopant and oxygen vacancies inside the fluorite structure will then greatly influence the ionic conductivity of the doped material at a given temperature and is the subject of intense research [3, 11-13]. It is thus of prime importance to study the evolution of the starting fluorite structure with the rate of dopant. Different dopant and vacancy arrangements have been considered for the doped CeO_2 structure. There are three basic defect types, the isolated defect (RE'_{Ce} and $V_O^{\bullet\bullet}$) the charged associated dopant-vacancy pair ($[RE'_{Ce}V_O^{\bullet\bullet}]^{\bullet}$) also called dimer and the neutral association in the Near Neighbour position (NN) of two RE'_{Ce} with one $V_O^{\bullet\bullet}$ ($[RE'_{Ce}V_O^{\bullet\bullet}RE'_{Ce}]^x$) also called trimer. The aggregation of those basic defects, when the doping cation and the oxygen vacancy concentrations are increased, generates some clusters which approach ~~more or less~~ the C-type RE_2O_3 structure (bixbyite). The presence of such defects can be

deduced from the results of experimental characterizations. Thus, Ohashi *et al.* [14] propose the presence of neutral trimers to explain the evolution of Ce-O and Gd-O distances with the doping ratio based on Extended X-Rays Absorption Fine Structure (EXAFS) spectrometry results. Deguchi *et al.* [15] also from X-Rays Absorption characterizations suggest that "*a basic structure in GDC is composed of 1–2* Gd^{3+} *adjacent to one oxygen vacancy, and this basic structure distributes randomly in ceria lattice*". Shibharte *et al.* [16] indicate from EXAFS data that for Sm-doped ceria dimer dominates while for Gd-doped ceria trimer is more than dimer. From the UV-Raman characterization Taniguchi *et al.* [17] propose for the Gd-doped system that isolated defects are mostly present for a low temperature synthesis (coprecipitation/200°C) and that after diffusion at higher temperature dimers form. Yamamura et al. [18] propose the presence of dimers and trimers for Sm-doped ceria at 573K from dielectric relaxation curves. Giannici *et al.* [19] are in favour of the presence of SmO_8 cubes and thus more in accordance with a random distribution of isolated defects for a low doping level. Koettgen and Martin [20] recently agree the random distribution of defects in Sm doped ceria at room temperature supported by a coordination number study extracted from EXAFS measurements. For the study of the structure evolution (X-Ray diffraction/Rietveld) with the dopant level Artini *et al.* [21] used a hybrid crystallographic structure where the dopants are distributed at random and the vacancies gradually order around them describing by this way the continuously passage from a pure fluorite structure to a pure C-type RE_2O_3 one. Calorimetric experiments lead Chen and Navrotsky [22] to suggest that the primary associates in CeO_2-$MO_{1.5}$ are neutral trimers with the oxygen vacancy in NN position relative to the doping cations.

The influence of the presence of the basic defects and their combinations on the structure and properties of ceria-based materials have also been extensively regarded using computer

modelling. Employing the Static Force Field simulation based on pair potential interactions it is possible to energetically probe the defect arrangements. Butler et al. [23] have first proposed an explanation of the trend of ionic conductivity with the doping cations ionic radii based on the basic defects binding energy calculation. Wei *et al.* [24] conclude that for Gd-doped ceria the Gd^{3+} ions are distributed randomly while it has been evidenced that the conformation of charged and neutral defects is highly dependent on the parameter set chosen for the pair potential interactions [25]. Other authors discuss the arrangement of larger clusters [26-29] employing different parameter sets. First principles simulation where electronic structure is considered has also been largely exploited to correlate the basic defect structure with the oxygen diffusion activation energy [30-34] or the reducibility of doped CeO_2 [35-37]. Those preceding simulations being static ones they are proceeded at 0 K. The influence of the temperature on the structure and properties of doped ceria is then introduced using Molecular Dynamics (MD) or Kinetic Monte Carlo (KMC) technics. Molecular Dynamics simulations lead to different results according to the parameter set used. Thus, for the Gd-doped ceria Inaba *et al.* [38] report that the system is more stable when Gd-Gd pairs are distributed at random inside the structure while Cui *et al.* [39] propose that the stability is improved when isolated Gd^{3+} ions are placed at random. Tarancon *et al*. [40] simulate the Gd-doped ceria structure distributing Gd^{3+} ions and oxygen vacancies at random while Hayashi *et al.* [41] and Huang *et al.* [42] prefer to distribute randomly the Gd-Gd pairs. In KMC simulations the starting structure is a randomly distributed one [43-45] or a non-random one resulting from a minimization procedure [13,46,47] with a preferred presence of associated defects.

To sum up, it seems difficult to be sure that a type of repartition is favoured over another one for a particular dopant even if recent works confirm the trend that Gd dopant attracts oxygen vacancy while Sm repels it. Indeed, Grieshammer *et al.* [13], Purton *et al.*[12] and Žguns *et al.*[48,49]

have shown the attraction/repelling property with simulations in accordance with experimental observations. In those studies, an equilibration step (Monte Carlo) is performed for a temperature T>1500K describing the structure of the doped ceria close to the thermodynamic equilibrium. This step is not necessarily present for the synthesis and/or operation at low or intermediate temperatures and different defect distributions (isolated defects and/or trimers) could then be expected. Thus Guizard *et al.* [50] obtained crystallized Gd-doped CeO_2 at a temperature as low as 150°C by a supercritical CO_2 aided sol-gel process and Kraynis et al. [51] assumed that both dopant and oxygen vacancies are distributed at random for doped ceria thin films due to the use of magnetron sputtering at 400°C.

The present work focuses on the study of doped CeO_2 fluorite structure at 298 K resulting from Molecular Dynamics simulations. We particularly pay our attention on the influence of the defects arrangement on the structural features as the lattice parameter, the ion-ion bond length and the ion coordination number. We then compare the simulation results to the available experimental data extracted from the literature. We have tested the Gd-doped and Sm-doped systems as they are the two systems considered as the best choice to reach the highest ionic conductivity [52-56]. Furthermore, the case of the co-doped ceria is investigated knowing that a controversy exists concerning the benefic effect or not of co-doping on the ionic conductivity. Indeed, some authors announce an improvement of the ionic conductivity by a synergetic effect due to co-doping [57-59] while others observe no improvement [60,61]. These two conclusions are also drawn from simulations with authors in favor of an enhancement of the ionic conductivity [62,63] and others observing no enhancement [64,65]. Therefore, the structure of the co-doped ceria has to be compared to the structure of the single-doped ceria to be able to detect if some structural modifications could be related to a modification of the ionic conductivity.

2. Simulation procedures

To perform the MD simulations, we employ the LAMMPS simulation code [66]. The NPT ensemble with zero external pressure is adopted and the Nosé-Hoover algorithm is used to control the temperature and pressure. The Ewald sum is applied to calculate the electrostatic energy. For each simulation the time step is fixed at 1 fs. The structure is first minimised (0 K Static Force Field) then an equilibration step is performed at the desired temperature during 7500 steps (7.5 ps). The results are then collected after the 250 ps of the final dynamics step.

The starting simulation supercell contains 8×8×8 CeO_2 fluorite unit cells with periodic boundary conditions. We study the doping of this structure with Gd, Sm and Gd/Sm (1:1) cations. For each doped system ($Ce_{1-x}RE_xO_{2-x/2}$) and each doping ratio (x=0, 0.05, 0.1, 0.15, 0.2, 0.25, 0.3) two dopant arrangements are examined. In the first arrangement (GdR, SmR, SGR) dopants and oxygen vacancies are distributed at random and in the second arrangement (GdN, SmN, SGN) these are the trimers ($RE'_{Ce}V_O^{\bullet\bullet}RE'_{Ce}$) that are distributed at random with RE the doping cation (Gd or Sm) in the nearest neighbour position relative to the oxygen vacancy. Those two configurations can then be viewed as two extreme cases. Obviously, a C-type like RE_2O_3 structure (with ordered and/or disordered vacancy distributions) will then be expected to be approached first by the aggregation of trimers which already contain one vacancy for two doping ions. In our opinion the interest of studying those two extreme cases comes from the fact that in the experimental samples the defects distribution could result of a mix of the R and N arrangements with different proportions of each one. A random distribution of dimers would also be an interesting arrangement to consider in order to study if the system behaves as an intermediate case between the R and N distribution.

For each system five structures are generated and the final result is averaged over those five structures. Then the structures are all different in their defect distribution and in the doping cation nature. Those arrangements are created using the Atomsk code [67]. The Molecular Dynamics simulations are carried out at 298 K. We label those simulations with first the doping level then the doping cation and third the arrangement, in this way the 20SGR simulation corresponds to Gd/Sm co-doped ceria in the random arrangement with x=0.2 ($Ce_{0.8}Gd_{0.1}Sm_{0.1}O_{1.9}$).

The pair correlation functions $g_{ij}(r)$ or Radial Distribution Functions (RDF) are determined for all ion pairs using the relation:

$$g_{ij}(r) = \frac{n_{ij}(r)}{4\pi(N_i N_j/V)r^2\Delta r} \qquad (2)$$

Where N_i and N_j are the number of ions in the cell with volume V, $n_{ij}(r)$ is the number of ij ion pairs present between the distance $r-(\Delta r/2)$ and $r+(\Delta r/2)$ with Δr=2.5pm in this study. For each simulation $g_{ij}(r)$ is calculated each 10000 steps and then averaged. The pair correlation first peak is always fitted by a log-normal function (3) as it is detailed in [68]. We use the log-normal function as defined in the *Fityk* program [69]:

$$y = h\exp\left\{-\ln(2)\left[\frac{ln\left(1+2b\frac{x-c}{w}\right)}{b}\right]^2\right\} \text{ and } FWHM = w\left(\frac{\sinh(b)}{b}\right) \qquad (3)$$

where h is the peak height, w the peak width, c the peak position, b the peak asymmetry parameter and FWHM the Full Width at Half Maximum.

For all the pairs the coordination number (CN) is obtained through the integration of the pair correlation function first peak.

In this work the short-range interaction is described by a parameterized pair potential model, here the Buckingham function:

$$E_{ij} = A_{ij} exp\left(-\frac{r_{ij}}{\rho_{ij}}\right) - \frac{C_{ij}}{r_{ij}^6} \qquad (3)$$

E_{ij} is the two-body interatomic potential and r_{ij} the distance between ions *i* and *j*. The parameters A_{ij}, C_{ij} and ρ_{ij} have to be determined in order to describe a specific ion-ion interaction. A cut-off distance of 13 Å is fixed for the short-range interaction and the cation-cation interaction is considered to be purely coulombic.

Knowing that the used parameter set largely influences the results of the Force Field (static or dynamics) calculations [25] we have chosen the set proposed by Huang *et al.* [42] by comparing some results with experimental data as described in our preceding work [68]. Those parameters are listed in Table S1 of the Supplementary Material.

We have limited our simulations in the composition range 0≤ x ≤0.3 for two reasons, firstly this is the range where the maximum of ionic conductivity is usually observed and secondly the used parameter set is not adapted to describe the structure of C-type RE_2O_3 systems (lattice parameter, thermal expansion, ...) [42].

3. Results and discussion

3.1. Lattice parameter

The lattice parameter of doped ceria is highly dependent on the local structure and more particularly on the cation-$V_O^{\bullet\bullet}$ arrangement at the atomic-mesoscale level. This arrangement will greatly influence the physico-chemical properties of the material as its density, ionic conductivity or catalytic activity. It is the reason why different models have been developed to link the value of the measured lattice parameter (X-Ray or Neutron diffraction) to the presence of local structures where cations and oxygen vacancies are associated in the defected fluorite lattice. This knowledge would then be useful to interpret the properties of the doped ceria. All those models

are based on the values of the room temperature cation and oxygen anion radii as determined empirically by Shannon and Prewitt [70] and later revised by Shannon [71].

In the model developed by Kim [72] the Vegard law is assumed to be valid and after a multiple regression analysis the following expression is proposed for the doped CeO_2 system:

$$a_{CeO_2} = 0.5413 + \sum_k (0.022\Delta r_k + 0.00015\Delta z_k) m_k \qquad (1)$$

with Δr_k the cation radius mismatch (r_k - r_h) between the dopant (r_k) and the host cation (r_h) both in eightfold coordination. Δz_k is the valency difference (z_k - z_h), and m_k is the mole percent of the kth dopant in the form of MO_x.

In their model Hong and Virkar [73] consider the oxygen vacancy as a specie and assign to it an ion radius. They thus determine the evolution of the lattice parameter of doped ceria ($Ce_{1-x}M_xO_{2-x/2}$) as follow:

$$a(x, r_M) = {}^{4}/_{\sqrt{3}} \times \left[x r_M + (1-x) r_{Ce} + (1 - 0.25x) r_O + 0.25x r_{V_O}\right] \times 0.9971 \qquad (2)$$

where r_M and r_{Ce} are the ionic radius of M and Ce in the coordination 8, r_{Vo} the oxygen vacancy radius and r_O the ionic radius of oxygen in coordination 4. By a fitting approach of experimental data, they determined r_{Vo} to be 1.164Å for the CeO_2-$MO_{1.5}$ solid solution.

Kim and Hong-Virkar in their models admit that the repartition of dopant is homogeneous in the fluorite lattice and they successfully tested them for x<0.3.

Another approach is to consider the r_{cation} evolution with the coordination number as it is defined by Shannon [70,71]. Then a single cation coordination number (the same for the host and the dopant) in a random distribution of dopant in the structure and two CN (one for the host and one for the dopant) for a non-random distribution are defined. In this view Nakamura [74] proposes a new model where the non-random distribution is connected to the preference of the oxygen

vacancies to be associated to the host or the dopant cation while no preference is assumed for the random distribution.

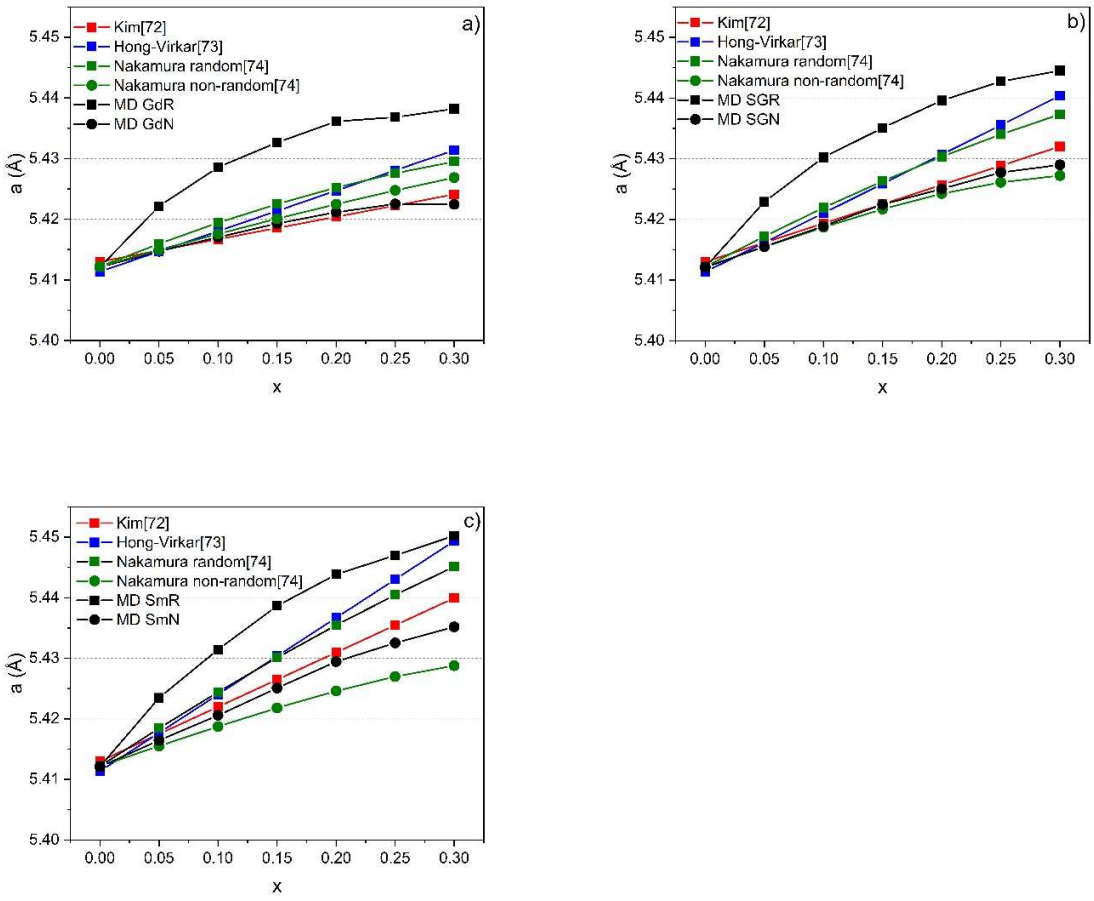

Fig. 1. Evolution of the lattice parameter of $Ce_{1-x}M_xO_{2-x/2}$ as a function of the composition according to the different models [72-74] and MD simulations. a) M=Gd; b) M=Gd/Sm; c) M=Sm.

In Fig.1 the different models are compared with the MD simulations for the Gd-doped, Sm-doped and Gd/Sm co-doped ceria. As indicated by the relations (1) and (2) the lattice parameter of the doped ceria varies linearly with x for the Hong-Virkar and the Kim models. The Nakamura models (random and non-random) reveal a non-linear relation between the lattice parameter and the doping level as it is the case for the MD simulations for the two defect configurations R and

N even if it appears more evident for the R configuration. This figure illustrates the non-equivalence of those models for the description of the lattice parameter evolution with the doping level. The Hong-Virkar model leads to results close to the Nakamura random one for the three systems mainly for $x \leq 0.2$ while the Kim model seems more in accordance with the MD simulation for the N configuration letting suppose that in the major part of the samples used for the Kim model (linear regression) the defects were distributed in the N arrangement. It is important to remind here that all those models are empirical and that only the Nakamura description and the MD simulations propose two kinds of defect arrangement. However, noticeable differences exist between the Nakamura models and the MD simulations. The random Nakamura model leads to lattice parameters lower than the MD Random (homogeneous) ones for the three systems while for the non-random (heterogeneous) model the results are slightly higher than the MD Neighbour ones for the Gd-doped ceria, quasi equivalent for the co-doped ceria and lower for the Sm-doped ceria. For the three systems the MD N line seems to be the closest of the other models at least in the x range [0-0.2].

We have then decided to compare the results of our simulations with experimental data available in the literature. This comparison is presented in Fig. 2 where all the diffraction patterns are acquired at room temperature. We then observe that the great majority of the experimental lattice parameters is comprised between the limits formed by the Random and the Neighbour Molecular Dynamics lines. Those experimental data spread over a large range and cannot be described by a single model as the Kim, the Hong-Virkars or the Nakamura one. The presented results can then be interpreted as resulting of a mix of R and N configurations in the experimental samples but it cannot be excluded that others factors also affect the value of the lattice parameter as misalignment of XRD set up, presence of impurities, non-stoichiometry or crystallite size.

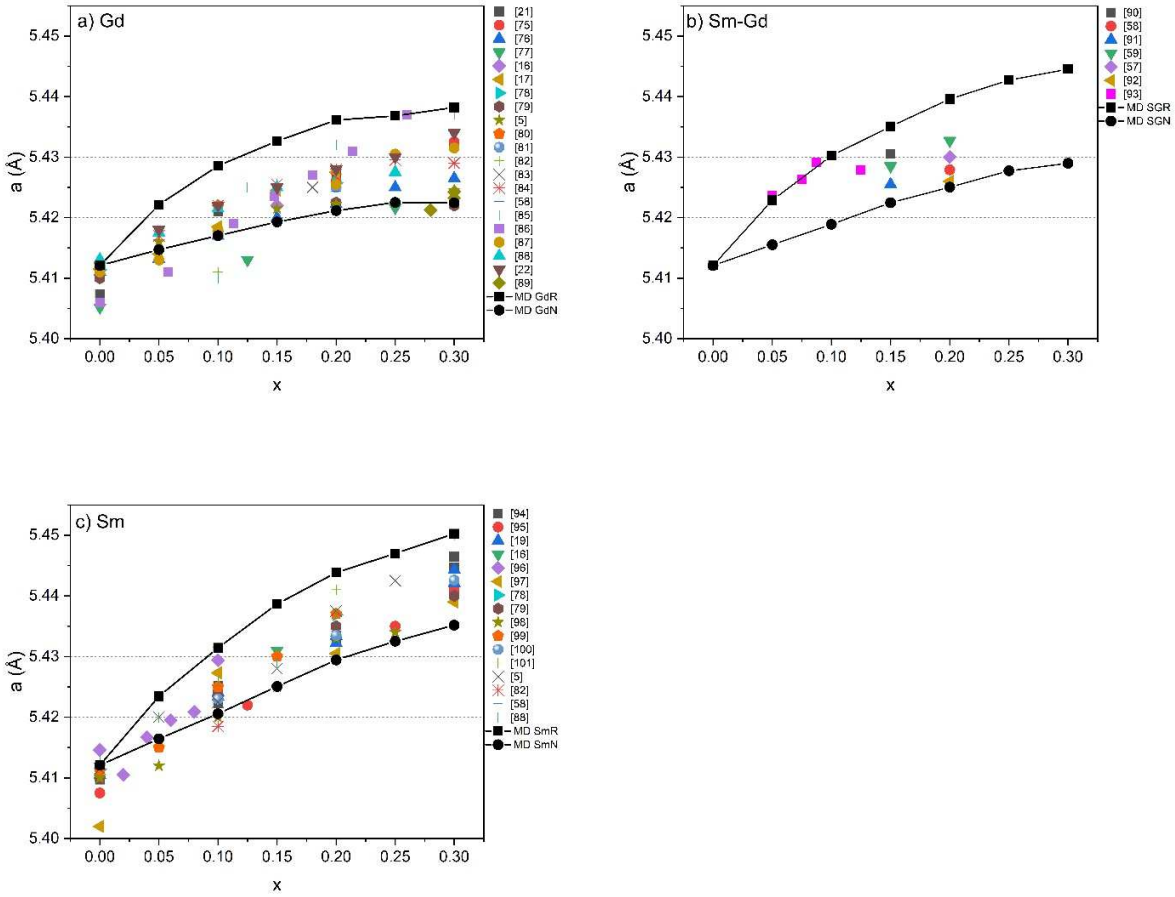

Fig. 2. Comparison of the MD lattice parameter results with literature data at 298 K. a) Gd-doped CeO_2 [5,16,17,21,22,58,75-89]; b) Gd/Sm co-doped CeO_2 [57-59,90-93]; c) Sm-doped CeO_2 [5,16,19,58,78,79, 88, 94-101]

Furthermore, the defect association/dissociation reactions may lead to the evolution of the lattice parameter with time and the equilibrium state could be attained only within several months [102]. All the changes in the lattice parameter of pure CeO_2 induced by the introduction of defects (doping cation, oxygen vacancy) and referred as chemical expansion could be the source of strain/stress and could lead to important damages in operating conditions [103,104]. In order to evaluate this defect induced lattice parameter change the chemical expansion coefficient α_c is introduced and defined as [103]:

$$\propto_C x = (\propto_M + \propto_V)x = \frac{a - a_0}{a_0} = \varepsilon$$

Where a_0 is the lattice parameter of the undoped CeO_2, a the lattice parameter of the doped ceria ($Ce_{1-x}M_xO_{2-x/2}$), ε the chemical expansion, α_M the part of the chemical expansion due to the cation radius change and α_v the part due to the introduction of oxygen vacancies inside the fluorite structure. α_c is then obtained by a simple linear fit of the evolution of ε with the composition. Those fits are performed for the MD simulations up to x=0.2 due to the high departure from linearity present beyond this value mainly for the R configuration. Based on the Hong-Virkar work [73] the empirical oxygen vacancy radius r_v can be deduced in a second step as described by Marrocchelli *et al*. [103]. In Table I are presented the results of the chemical expansion analysis along with the values of the oxygen vacancy radius deduced from the Marrocchelli *et al.* and the Nakamura methods [74]. The chemical expansion coefficient is lower for the N than for the R configuration meaning a less mechanical perturbation when foreign ions are introduced in the fluorite structure close to each other and in the NN position relative to the oxygen vacancies**.** The value of experimental α_c could then be an indication for the distribution of the dopant inside the fluorite structure with the higher the coefficient the more random the distribution. The chemical expansion coefficient also depends on the doping ion radius with the Sm^{3+} cation (1.079Å) leading to higher α_c than the Gd^{3+} cation (1.053Å). The determination of this coefficient from the experimental data used in Fig. 2 yields values in the range [0.01-0.02] for the Gd-doped materials and in the range [0.02-0.028] for the Sm-doped materials with no correlation with the synthesize method (solid state, precipitate, gel combustion…).

Table I
Chemical expansion α_c and oxygen vacancy radius r_v for the different structures.

structure	α_c	r_v (Å) from Marrocchelli *et al.* model [103]	r_v (Å) from Nakamura model [74]
GdR	0.01691	1.2069	1.5229
GdN	0.00796	1.1228	1.5221
SmR	0.02508	1.1797	1.5257
SmN	0.01601	1.0945	1.5227
SGR	0.02018	1.1857	1.5243
SGN	0.01182	1.1071	1.5226

For a same doping system r_v calculated using the Marrocchelli *et al.* method is different for the random and the non-random arrangement. However, if we average r_v over the six present structures the result (1.149Å) is close to the one experimentally found by Hong and Virkars [73] (1.164Å) and Marrocchelli *et al.* (1.169Å) [103] for the host CeO_2. ~~letting suppose a mean mixed arrangement among the samples used by those authors for the fitting procedure~~. We can then suppose that the samples used by those authors for the fitting procedure present in average a defect distribution between a N and a R distribution. Another approach for the determination of r_v is proposed by Chatzichristodoulou *et al.* [104] by linking the Kim and the Hong-Virkar models (equation (1) and (2)). In this approach and conversely to the Marrocchelli *et al*. and Hong-Virkar models r_v is a function of the doping cation radius. Adopting this third model very close values around r_v=1.10Å are found for the three doping systems due to the near value of their cation radius. Nakamura model [74] also allows to calculate an oxygen vacancy radius that depends not only on the dopant radius but also on the arrangement and on the doping level. In this case (Table I) the vacancy radius values obtained for the different structures studied here are more homogeneous. The main discordance between all those models being that the oxygen vacancy radius is higher than the oxygen one for Nakamura while it is always lower for the others authors.

The Table I also indicates that the Gd/Sm co-doped structure seems to behave as a simple average of its two components.

A way to avoid the contribution of the oxygen vacancies on the lattice parameter change is to plot the mean atomic volume (cell volume/number of atoms) as a function of the composition as proposed by Artini *et al.* [94,105]. Those plots for the three systems then show a linear trend over the composition range [0-0.3] indicating the formation of a solid solution with a reliability factor always slightly higher for the N configuration and an increasing slope in the sequence GdN, SGN, SmN, GdR, SGR, SmR doped ceria (Fig. S1 of the Supplementary Material).

3.2. Bond length

The introduction of trivalent rare earth cations in place of the Ce^{4+} cations in the fluorite CeO_2 structure also greatly modifies all the bond lengths between ions due to the size of the rare earth cation itself and to the extraction of oxygen ions. Distortions appear around the foreign cations and the oxygen vacancies and thus break the existing symmetry. Those distortions not only intuitively increase with the doping ratio but are also related to the way the point defects are geometrically distributed. MD simulation is then adapted to reveal the effect of the distortions for the R and N distributions on the Radial Distribution Functions. We present in Fig. 3a the evolution of the M-M (M=Ce, RE) bond length with the doping level for the Gd-doped ceria.

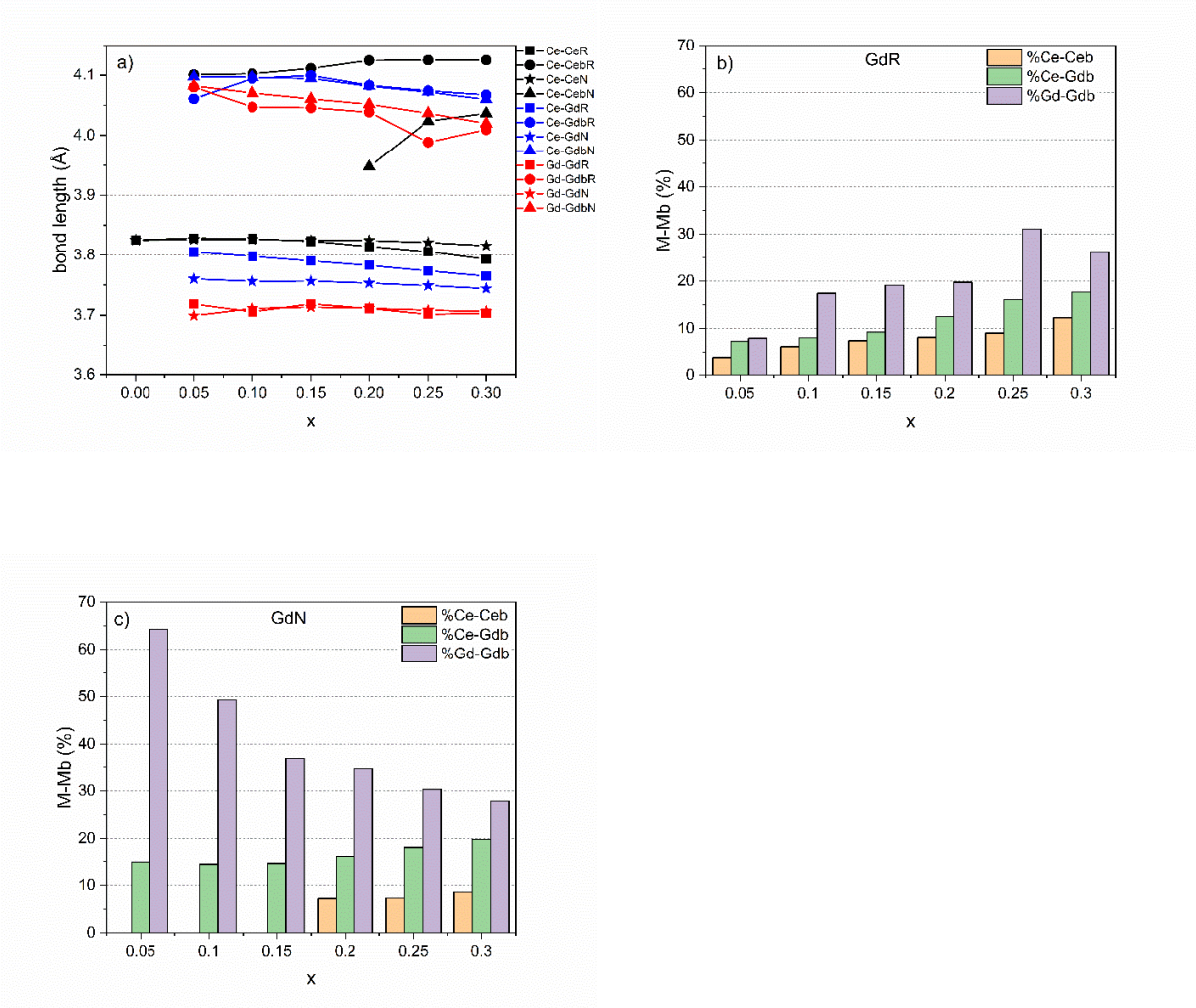

Fig. 3. a) Evolution of the M-M bond lengths with the composition for the Gd-doped CeO_2 system at 298K. Ratio of the M-Mb RDF peak area over the total peak area (M-M+M-Mb) as a function of the composition. b) R configuration; c) N configuration.

At room temperature the M-M RDF first peak can be decomposed into two components for all the systems (Fig. S2). We call this second component M-Mb. Those two components testify to the presence of local lattice distortions and/or REO_x clusters due to the introduction of doping cations and oxygen vacancies. In this study we consider the REOx clusters as clusters comprising dopant cations, oxygen anions and oxygen vacancies (not necessarily perfectly ordered) having a structure approaching the C-type RE_2O_3 one, those clusters are then similar to the distorted C-type regions as defined by Coduri *et al.*

[95]. Such split has been experimentally observed for the M-M bond length. Artini *et al.* [94] using a hybrid F-C structure for their X-Ray diffraction Rietveld refinements observe a split of the M-M distance beyond x=0.2 for Gd-doped ceria and beyond x=0.3 for the Sm-doped ceria. Scavini *et al.* [77] for the $Ce_{1-x}Gd_xO_{2-x/2}$ structure and Coduri *et al.* [95] for the $Ce_{1-x}Sm_xO_{2-x/2}$ structure detect the presence of two M-M lengths since x=0.125 using à biphasic model for the fit of the Pair Distribution Function (PDF) at short distances (1.5Å<r<6Å). Recently Kraynis *et al.* [51] using an RMC-EXAFS simulation also proposed the bimodality of the Sm-Ce lengths since x=0.05.

In the C-type Gd_2O_3 structure two main Gd-Gd distances exists, one around 3.6 Å and the other around 4.07 Å [12,68,77] giving rise to two well separated RDF peaks. The two lengths of the M-M bonds in Fig. 3a are divided in 3 groups corresponding to the Ce-Ce bond (in black) Ce-Gd bond (in blue) and the Gd-Gd bond (in red). The evolution of those lengths with the composition has to be correlated with the evolution of the percentage of the M-Mb bond displayed in Fig. 3b and Fig. 3c for the R and N configurations. This percentage is calculated through the ratio of the M-Mb RDF peak area over the total area (M-M +M-Mb). Ce^{4+} ions form the major part of the metal ions inside the lattice, the Ce-Ce bond network could then be viewed as the backbone of the structure. For the R configuration this bond is affected since the introduction of doping ions (x=0.05) as it is evidenced by the appearance of the Ce-Ceb component (Fig. 3a and Fig. 3b) and as it has been unveiled earlier from hybrid Monte Carlo simulations [12]. Contrariwise for the N configuration this component is not present at low doping ratio, indeed the distortions only localized around the Gd-Gd pairs affect a minor part of the backbone. We note in Fig. 3a that for each type of M-M bonds the position of the two components does not evolve in a large extent with the composition. The two components of the Gd-Gd bond are the closest to the ones of the C-type Gd_2O_3 and the Ce-Ce bond components the most distant with the lowest component quasi the same as in undoped CeO_2. Furthermore, no large gap can be noted concerning the M-M (or M-Mb)

positions between the N and R configurations meaning that when the split occurs two populations are created and positioned at fixed sites. The percentage of the Ce-Ceb (Fig. 3b and Fig. 3c) component increases monotonously with the doping level for the two tested configurations. For the Ce-Gdb bond the percentage increases with the doping level for the R configuration while it remains constant up to x=0.15 for the N case meaning that till this level the same proportion of the Ce cations nearby the clusters formed by the Gd-Gd pairs is affected.

The second component of the Gd-Gd RDF first peak evolves inversely up to *x*=0.2 in the case of the N and R configurations. For the N configuration the Gd-Gdb component his high at low doping ratio (*x*=0.05) and diminishes with the composition up to *x*=0.2 while for the R configuration it increases from *x*=0.05 up to *x*=0.2. In the case of the N arrangement ($Gd'_{Ce}V_O^{\bullet\bullet}Gd'_{Ce}$) defects are distributed at random without large interaction between them and for the R arrangement the few Gd-Gd pairs randomly generated in the structure are not mainly in the vicinity of an oxygen vacancy giving rise to different components weight in the Gd-Gd first shell peak. We have to note that in C-type RE_2O_3 (RE=Gd, Sm) the percentage of each bond is close to 50%. It is interesting to note here that Scavini *et al.* [77] for the Gd-doped ceria and Coduri *et al.* [95] for the Sm-doped ceria calculate an increase of the M-Mb component with *x* but without the ability to differentiate the two cations (Ce^{4+} and RE^{3+}) rendering the comparison with the present simulations not straightforward. Nevertheless, if we consider that a major part of the M-M bonds corresponds to the Ce-Ce bonds (for $0<x\leq0.3$) and to a less extent to Ce-Gd bonds, the M-Mb component increases up to [0.1-0.2] both in the present simulations (fig.3) for the two configurations and in the pdf analysis [77,95]. The same trends in our simulations are observed for the Sm-doped system (Fig. S3). The analysis of the co-doped ceria M-Mb bonds leads to more complex results due to the presence for the two configurations of six different bonds each with two

components. However, results of such analysis are presented in Fig. S4 and high similitude is noticed with the superposition of the Sm-doped and-Gd doped ceria results with an addition of a Sm-Gd bond.

In Fig. 4 is displayed the evolution of the M-O and O-O bond lengths ($d_{M\text{-}O}$ and $d_{O\text{-}O}$) with x for the Gd-doped ceria. Inversely to what it is intuitively expected the Ce-O and Gd-O bond lengths decrease with increasing the doping rate. This evolution has already been noted experimentally [14-16,19,20,51,75,77,95,106,107] and using simulations [12,38,39] for the Gd-doped and Sm-doped ceria.

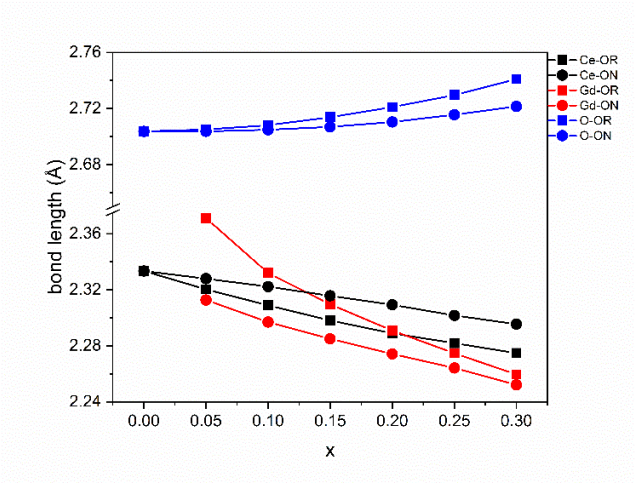

Fig. 4. Evolution of the M-O and O-O bond lengths with x for the $Ce_{1-x}Gd_xO_{2-x/2}$ structure.

The contraction of the M-O bond length is related to the rise of oxygen vacancies suggesting a displacement of the oxygen ions surrounding the vacancy towards this empty site thus decreasing the average cation-oxygen distance [14,20,38] mainly when two foreign cations (Gd or Sm) are in NN position relative to the vacancy (N configuration). This contraction is then different for the Ce-O and Gd-O bond length as it is also different in the case of the R and N configurations. In the same way as what was described previously for the Ce-Ce bonds, the major part of the Ce-O bonds in the N configuration is not influenced by the presence of the localized REOx clusters explaining why the contraction is less effective than in the case of the R configuration. The random distributed arrangement

leads to a Gd-O length higher than the Ce-O one till x=0.2 (till x>0.3 for the Sm-doped ceria see Fig. S5a) while for the neighbour arrangement the Gd-O length is always lower. However, the R and N d_{Gd-O} curves seem to join for x> 0.3 where the structures tend to become similar at least in a point of view of the REOx cluster number. The evolution of the M-O bond length for the co-doped system (Fig. S5) shows no noticeable difference comparing to a simple superposition of the evolution of the two singly doped lattices. Experimental data extracted from EXAFS acquisitions always results in d_{Gd-O} and d_{Sm-O} > d_{Ce-O} [14,15,19,75,51,106,107]. The discrepancy between our results and the EXAFS data could arise from several origins: the accuracy of the experimental data analysis (parameter correlations, model dependency of the fitting process), the samples studied experimentally are all in favour of a R configuration and/or the empirical potential parameters used in this study are not perfectly adapted for the description of the evolution of the M-O bond lengths [25].

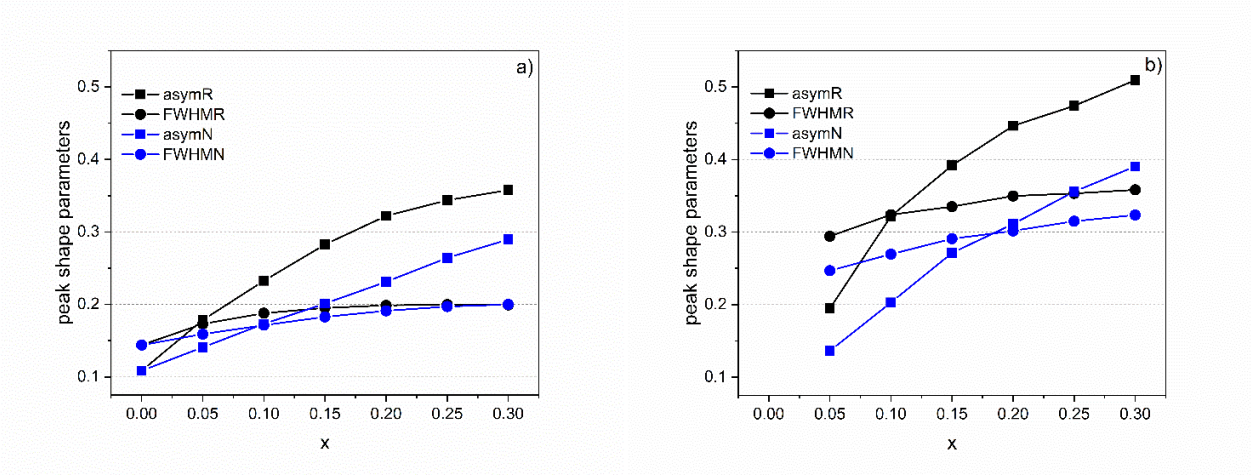

Fig. 5. Evolution with x of the peak shape parameters width (*FWHM*) and asymmetry (*b*) of the log-normal RDF first peak for the R and N configurations. a) Ce-O bond length, b) Gd-O bond length.

In this study the RDF first peak is always described by a log-normal distribution (see relation (2)) in order to take the peak asymmetry (*b*) into account [68], it is thus interesting to study the evolution of this parameter both with the peak width (FWHM) as a function of the composition as it is shown in Fig. 5

for the Gd-O and Ce-O first shell. Those two parameters reflect the rise of disorder around the metal cations. For the Ce-O bound the FWHM does not evolve in a large extent with the composition for the two configurations certainly indicating that the major part of those bounds is localized within this range (around the mean position). Contrariwise the peak asymmetry moderately increases letting suppose the creation of some new bond length populations at higher distances from the mean length. The N configuration is less impacted by this asymmetry because this perturbation is located near the $(Gd'_{Ce}V_O^{\bullet\bullet}Gd'_{Ce})$ defects where a minor part of the total Ce-O bonds is positioned while for the R configuration more Ce-O bonds are close to the Gd^{3+} cations and oxygen vacancies. It can then be considered that the disorder around the Ce^{4+} cations is present but moderate and in average higher for the R than for the N configuration. Both the FWHM and the asymmetry parameters of the Gd-O RDF first peak are larger than the Ce-O ones implying a higher distortion around the Gd^{3+} cations. The rise of those parameters is also greater for $d_{Gd\text{-}O}$ than for $d_{Ce\text{-}O}$. Thus, the more the foreign cations are added (the more the $V_O^{\bullet\bullet}$ are created) the more the distortion is present at the vicinity of Gd^{3+} cations. However, the Fig. 5b points out that for the N configuration the shape parameters (*b*, FWHM) are the lowest. Thus, the disorder is less important in this configuration surely due to the building of some clusters having a C-type phase structure where the Gd-O distance is more constrained. In Fig. S6 the evolution of the shape of the asymmetric Gd-O RDF first peak for the R and N configurations can be visualized and compared. Very similar results are obtained for the Sm-doped system as it is also the case for the co-doped system (Fig. S7 and Fig. S8).

The evolution with x of $d_{O\text{-}O}$ is shown in Fig. 4 and reveals a rise in all the composition range in correlation with the increase of the lattice parameter. This rise has been already evidenced by MD simulations [12,38,39,41] while to the best of our knowledge no experimental confirmation has been published nor by EXAFS or by pdf extracted from neutron scattering for the present systems. Only

Coduri *et al*. [108] for the system Y-doped CeO_2 and from neutron scattering acquisitions show that the O-O distance does not follow the trend of the lattice parameter (contraction with x). We can also note that Kraynis *et al.* [51] observe the evolution of the O-O distance with the doping rate for the Y doped and Sm-doped ceria films concluding to a decrease and an increase for the two systems respectively. The N configuration gives rise to O-O distance lower than the R configuration as it was also the case for the lattice parameter evolution. More interesting than this evolution is the pair correlation function ($g_{O\text{-}O}$) change with x in the range [2Å-5Å] extending the analysis beyond the first shell environment. In Fig. 6 is presented the O-O pair correlation function $g_{O\text{-}O}$ for CeO_2, C-type Gd_2O_3 obtained from the Buckingham parameter set listed in table S1 and $Ce_{0.7}Gd_{0.3}O_{1.85}$ (R configuration) up to 5.2 Å. The CeO_2 fluorite structure requires three peaks labelled 1,2 and 3 for the description of $g_{O\text{-}O}$, for the Gd-doped ceria a fourth peak is added (labelled 4) and for the C-type Gd_2O_3 structure a fifth peak becomes necessary. In each case the first peak is fitted with a log-normal function and the others with gauss functions [68]. The presence of the peak 4 for the doped ceria indicates a new site position for the oxygen anion and reflects, here again, the perturbation due to isolated Gd^{3+} and $V_O^{\bullet\bullet}$ and also to the REOx clusters generated inside the fluorite structure. This new site position thus reveals the distortion of some MO_8 cubes inside the lattice. This peak appears since the lowest doping ratio (x=0.05) for the two configurations and whatever the doping system (Gd, Sm, Gd/Sm). For each doped system we have next calculated the ratio $A=100*A_4/(A_1+A_2+A_3+A_4)$ with Ai being the area of the peak i. This ratio is then considered as an indicator of the disorder existing inside the structure.

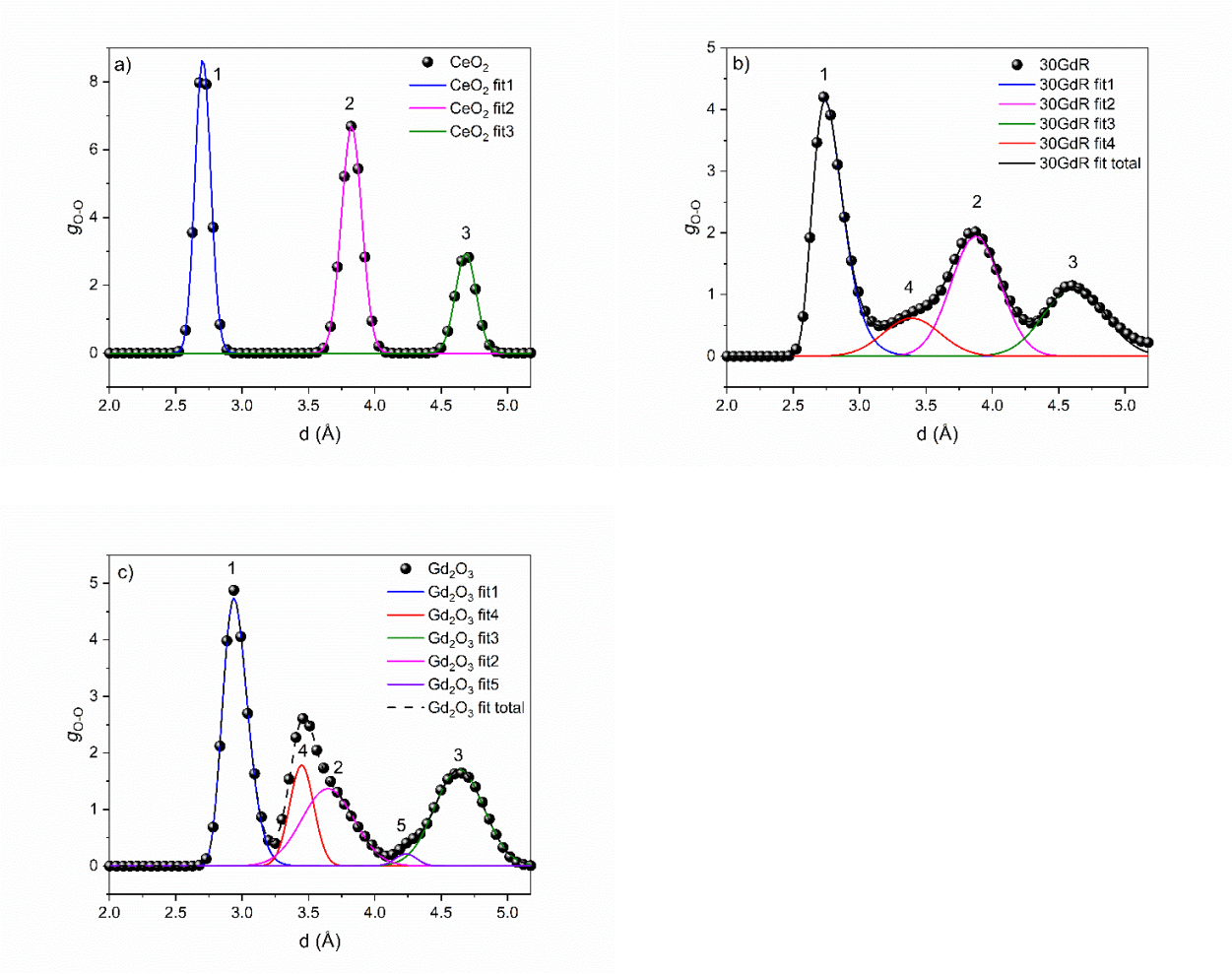

Fig. 6. O-O pair correlation function for a) CeO_2, b) $Ce_{0.7}Gd_{0.3}O_{1.85}$ (30GdR) and c) C-Gd_2O_3.

In Table 2 are grouped the results of such calculations along with the FWHM of the peak 4. We observe the extreme similarity of the results for the three doped systems meaning that the modification of the structure occurs in a same way for those systems. The *A* ratio and the FWHM increase for all the doping systems and the two defect configurations confirming that the disorder settles down at the local scale in the fluorite structure. The R configuration leads to higher *A* ratio due to the fact that more O-O pairs are concerned by the disturbance coming from the random introduction of the vacancies and foreign cations. For the N configuration the O-O pairs that are mainly affected are those around the $(RE'_{Ce}V_O^{\bullet\bullet}RE'_{Ce})$

clusters and consequently the calculated *A* ratio is lower. The FWHM are also lower for the N configuration suggesting that the distance of the corresponding O-O pairs is more stable as it could be the case in the C-type phase structure. The preceding remarks are corroborated by the lower asymmetry parameter and FWHM of the first lognormal peak for the N arrangement.

Table 2
Area ratio *A* and FWHM (Å) for the peak 4 of the O-O pair correlation function.

	Gd				Sm				Sm-Gd			
	Random		Neighbor		Random		Neighbor		Random		Neighbor	
x	*A*	FWHM	*A*	FWHM	*A*	FWHM	*A*	FWHM	*A*	FWHM	*A*	FWHM
0.05	1.6	0.32	0.97	0.23	1.5	0.33	0.9	0.24	1.6	0.34	0.95	0.23
0.1	3.3	0.41	1.9	0.25	3.0	0.35	1.8	0.26	3.1	0.36	1.8	0.25
0.15	4.3	0.37	3.1	0.31	4.1	0.35	2.9	0.31	4.3	0.37	2.9	0.31
0.2	5.8	0.40	4.3	0.38	5.6	0.39	4.1	0.38	5.5	0.37	4.2	0.37
0.25	7.5	0.43	5.7	0.41	7.2	0.42	4.9	0.38	7.5	0.42	5.3	0.39
0.3	11.5	0.53	6.6	0.42	10.9	0.51	6.2	0.41	11.1	0.50	6.1	0.39

3.3. Percolation concept

As it has been expressed all along this study REOx clusters are generated inside the structure when foreign cations and oxygen vacancies are introduced. Those clusters differ in their number, size and shape which depend on the doping ratio and on the arrangement adopted for the introduction of the foreign cations and oxygen vacancies. As proposed by Purton *et al.* [12] and with the assistance of the Ovito [109] and Vesta [110] softwares we have created a bond between two foreign cations when there are in the NN position from each other ($d_{RE\text{-}RE} < 4.5$Å) and called those entities "RE groups" which in a first approximation can be linked to the C-type RE_2O_3 clusters. Thus, the analysis of those groups relying on the sole starting arrangement is valid for the three doped systems. Examples of such representations are given in Fig. 7 for the 5SmR, 5SmN, 30SmR and 30SmN structures where the Ce^{4+} and O^{2-} ions have been omitted.

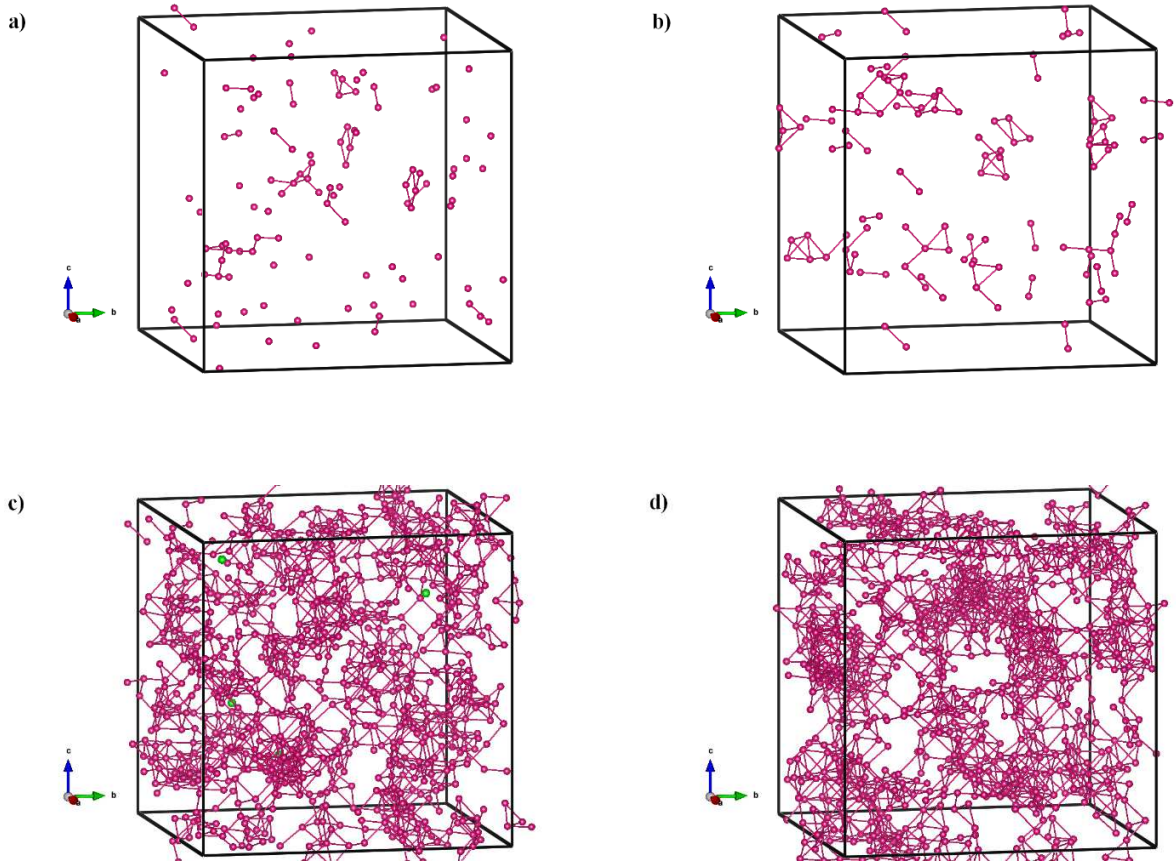

Fig. 7. Snapshots of the RE groups (RE=Sm) for a) 5SmR, b) 5SmN, c) 30SmR (in green isolated Sm cations), and d) 30SmN.

The first outcome of this depiction is the presence of isolated RE cations in the R configuration up to x=0.3. We also note that some small RE groups are already visible for x=0.05 in the R configuration while they are the sole present in the N configuration. The main difference is that in the N configuration, due to the low oxygen diffusivity at room temperature, vacancies are situated in the vicinity or inside the RE groups letting suppose a more C-type like structure. Those groups can then be viewed as a having fluorite structure with a partial ordering of oxygen vacancies or as dopant and oxygen vacancy rich aggregates with distorted C-type phase [95,111]. In order to quantify the number (size) distribution *S* of the RE groups we have calculated for each group length (number of connected RE cations) the percentage of RE cations involved in such group over the total RE cation number. The distributions thus

calculated and presented in Fig. 8 are then the arithmetical means over the five structures generated for each system. At low doping concentration (Fig. 8a and Fig. 8b) the major part of the RE cations belongs to small groups with near 50% (x=0.05) and 25% (x=0.1) single cations for the R configuration and the largest group with *S*=12 (x=0.05) and *S*=40 (x=0.1) for the N configuration. As x increases (x=0.15-0.2) the size distribution gradually evolves. For x=0.15 the major part of RE cations still belong to low size groups (R) or are more or less homogeneously distributed (N) while for x=0.2 high size groups encompass the majority of the dopants whatever the arrangement. For the highest doping ratio two well separated distributions (bimodal) appear where a tiny part of the RE cations are always inside low size groups for x=0.25 and the quasi-totality inside large size groups for x=0.3. For all those distributions we observe that introducing the same number of dopants the largest group is constantly obtained when those dopants are distributed as RE-RE pairs. We also note that the R and N distributions become more and more similar with the raise of x.

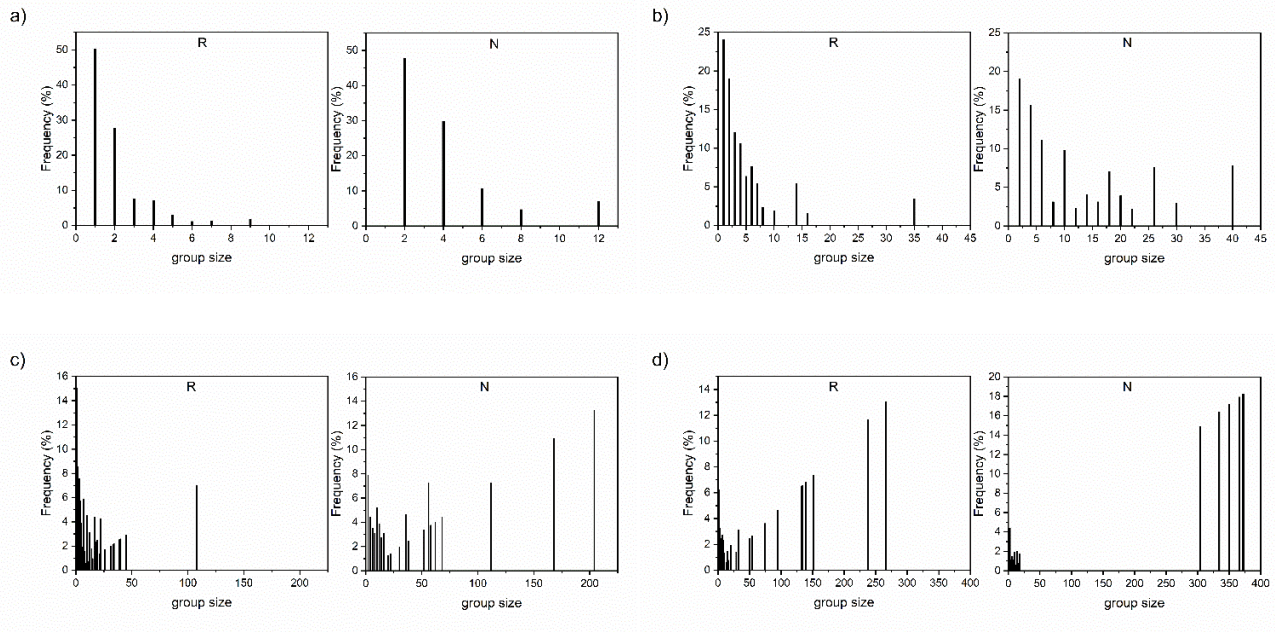

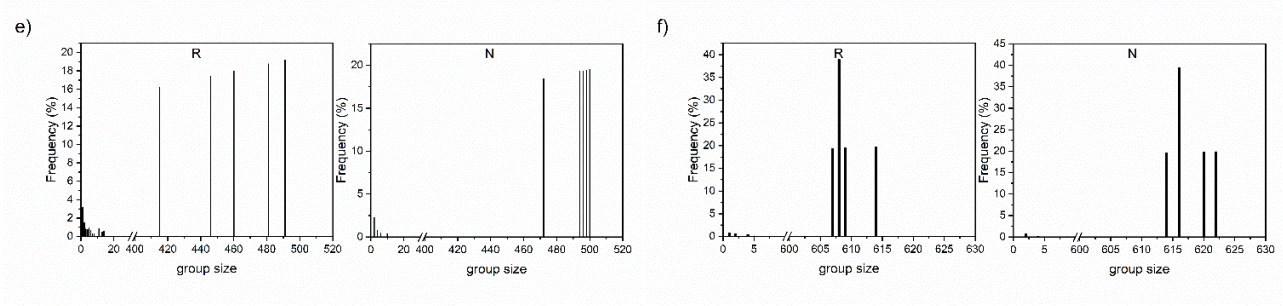

Fig. 8. Distribution of group size (*S*) for the two defect configurations a) x=0.05, b) x=0.1, c) x=0.15, d) x=0.2, e) x=0.25, f) x=0.3.

The percolation theory has been employed in a large field of application, from geology to biological systems [112] to model and explain a wide variety of phenomena. In this theory the percolation threshold is the main parameter linked to an abrupt change of properties of the system.

Concerning the doped ceria materials, the percolation threshold concept has been adopted by some authors to discuss the passage from the fluorite to the C-type RE_2O_3 structure in the ceria doped system. Artini *et al.* [94,105] for the Gd and Sm-doped ceria and based on high resolution X-Ray Diffraction (synchrotron radiation) results treated with a hybrid crystallographic structure proposed a x=0.5 threshold. This value then corresponds to a passage from the F-based matrix with embedded C-based microdomains to a C-based matrix embedding F-based microdomains and is similar to the site percolation threshold of a 2D square lattice. Scavini *et al.* [111] and Coduri *et al.* [95] situate the percolation threshold of the dopant and oxygen vacancy rich aggregates with distorted C-type phase (called nano droplets) around x=0.31(site threshold for a 3D simple cubic lattice) for the Gd-doped and Sm-doped systems. Those studies conclusions are then mainly supported by X-ray Rietveld, Whole Powder Pattern Fitting and pdf (biphasic model) results. Meyer *et al.* [113] using MC simulation and based on the simple cubic oxygen (vacancy) sublattice proposed some percolation threshold ranges according to different vacancy-cation environments and interactions. In this last study, where doping

cations are distributed at random, the percolation theory is designed as essential to explain the evolution of the ionic conductivity. We propose to study hereafter the percolation theory applied to the Ce sublattice with the influence of the defect distribution on the percolation threshold.

The Ce sublattice in CeO_2 is a FCC lattice which has been largely studied in the frame of the percolation theory. This theory [114] tells us for this lattice that the site percolation threshold is attained for a site critical probability P_{cs}=0.198 meaning that when the site occupation is distributed at random (R configuration) the percolation occurs around x=0.2. In the present study, we observe that over all the structures created a spanning group is never present for x=0.15 in the case of R configuration while for x=0.2 such a group with a is loosely branched structure is evidenced in ~ 53% of cases in accordance with the site theoretical threshold of a FCC lattice. For the N configuration a percolating group is present in ~ 27% of cases for x=0.15 and always present with a highly branched structure for x=0.2. Examples of percolating RE groups (R and N configurations) can be visualized in Fig. 9 for x=0.2. We can then conclude that the distribution of foreign cations for the N configuration leads to a site percolation threshold lower than x=0.2 in a range [0.1-0.2] where the ionic conductivity usually starts to decrease.

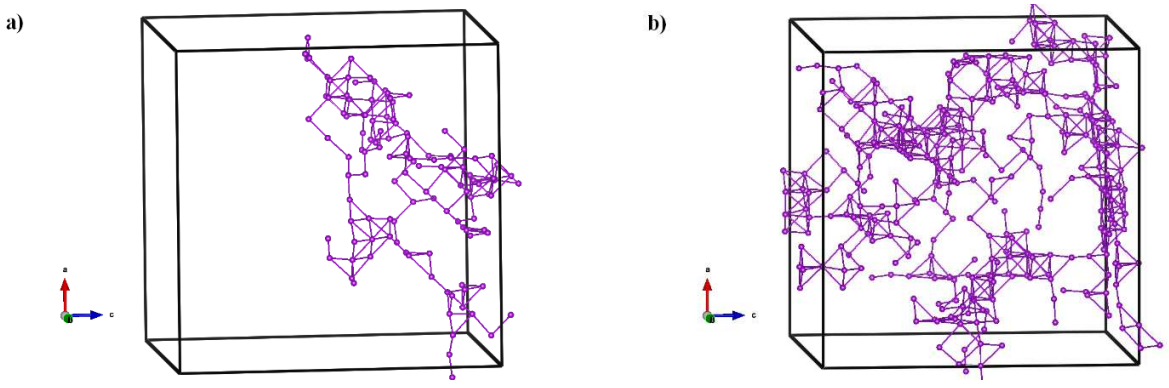

Fig. 9. Example of the percolating RE group for the composition x=0.2. a) R configuration, b) N configuration

The RE groups could only be viewed as C-type clusters if is they contain oxygen vacancies. Then the aforementioned observations have to be linked to the evolution of the metal cation coordination number (CN) for the first shell as depicted in Fig. 10 for the Gd-doped ceria. This figure, depending mainly on the distribution of defects, is similar for the Gd, Sm-doped and Gd/Sm co-doped systems. We note that only a slight difference exists between the R and N configurations for the CN(Ce-Ce) and CN(Ce-O) while the gap is larger for the CN(Ce-Gd) and CN(Gd-O) due to the initial distribution of defects and to the low temperature (298 K) avoiding a significant metal and oxygen diffusion even if some oxygen jumps are detected. For the Ce-O, Gd-O and Sm-O coordination numbers the available experimental data spread over a large range as it is summarized in Table 3 (and Fig.S9). The discrepancies appearing in this table arise from the technique employed (EXAFS, Raman), the data treatment, and the sample synthesis way. Among all those results only Giannici *et al.* [19] find a higher CN for the doping cation than for the host one, Deguchi *et al.* [15], Nitani *et al.* [106] and Yoshida *et al.* [60] conclude that oxygen vacancies are mainly situated in the first shell of the dopant. In Fig.10a the two dashed lines illustrate the theoretical evolution of CN for a random distribution of defects in accordance with R configuration results. The low gap between CN(Ce-O) and CN(Gd-O) for the R configuration is also in accordance with a theoretical random distribution visualized by the line CN=8-2x. However, we observe a departure from this theoretical line with CN(Ce-O) slightly over this line and CN(Gd-O) below this line. This non-perfect match confirms that even at room temperature (298K) vacancies could diffuse and/or relax with a preferred location close to the Gd cations (NN). ~~The non-perfect match between this line and the MD simulations is probably due to the non-sufficient number of the generated R structures~~. The N configuration is then characterised by a larger gap between the Ce-O and Gd-O coordination numbers than in the case of the R configuration. This gap ~~Those trends are~~ is also ~~described~~ evidenced by the Nakamura non-random model [74] and deduced from Metropolis Monte Carlo simulations [13]

but with a value ~~an~~ intermediary ~~lower~~ ~~gap~~ between ~~CN(Ce-O) and CN (Gd-O) than~~ the ones found in the present study for the R and N configurations.

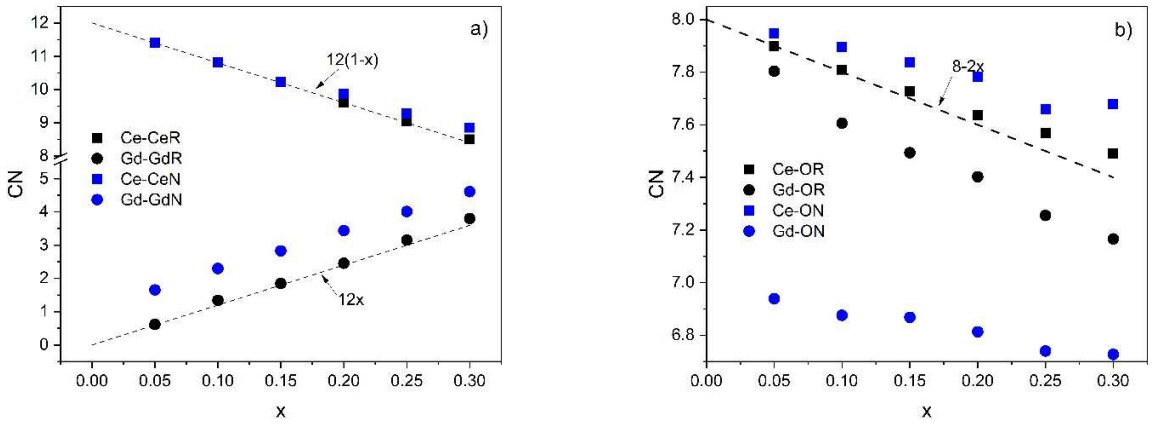

Fig. 10. Evolution with x of the coordination number (CN) for the N and R configurations. a) M-M; b) M-O.

It is noteworthy to point out that the main experimental data only concern the first shell of cations and/or do not allow to distinguish between CN(Ce-Ce) and CN(Gd-Gd) for the second shell only treating by this way the CN(Ce-Ce/Gd) [14,16,19,33,106,107,115,116] which renders the comparison with the present MD results not straightforward for the analysis of these cations second shell. However, Deguchi *et al.* [15] using "*a multiple data set fit*" separate the CN(Ce-Ce) and the CN (Gd-Gd) and conclude to the decrease of CN(Ce-Ce) with x while CN(Gd-Gd) remains constant and around 1 in the range [0.05-0.3]. From Fig. 10 and concerning the cations second shell the same rising (Gd-Gd) and decreasing (Ce-Ce) trends are evidenced for the two arrangements. The higher CN(Gd-Gd) denoted for the N configuration is the signature of more compact groups with a highly branched structure. Furthermore, as it is described by Kirkpartick [117] and McLachlan [118], at the percolation threshold the critical average number of bonds per site n_c which corresponds to the coordination number (CN) is invariant and only depends on the dimension d of the lattice. Thus, for a 3D lattice (d=3), n_c ~ d/(d-1) ~ 1.5 and this

value, in the present study, is reached for CN (Gd-Gd) till x=0.05 for the N configuration and in the x range [0.1-0.15] for the R configuration. This second way to localize the percolation threshold then confirms that the percolation is attained first for the neighbour distribution.

Table 3: Experimental data concerning CN(Ce-O) and CN(M-O) with M=Gd or Sm

x	CN(Ce-O) *Gd-doped*	CN(Ce-O) *SG-doped*	CN(Ce-O) *Sm-doped*	CN(Gd-O)	CN(Sm-O)
0.05	7.75 +/- 0.5 [15] 7.4 [120]		7.9 +/- 0.1 [20]	7.4 +/- 0.5 [15] 7.1 [119]	
0.1	7.65 +/- 0.5[15] 6.8 [119] 7.6 +/- 1.5 [120]		7.85 +/- 0.1 [20] 7.8(constrained) [19] 7.83 [106]	7.1 +/- 0.5 [15] 6.9 [119] 6.7 +/- 0.1 [115]	6.7 +/- 0.1 [115] 8 +/- 0.2 [19]
0.15	7.84[16]	7.2 [116]	7.75 +/- 0.1 [20] 7.52 [16]		
0.2	7.25 +/- 0.5 [15]		7.77[106] 7.5(constrained) [19] 7.65 +/-0.1[20]	6.65 +/- 0.5 [15] 6.5 +/- 0.1 [115]	7.17 [106] 7.9 +/- 0.2 [19] 7.2 [60] 6.7+/-0.1 [115]
0.25			7.4 +/- 0.1 [20]		
0.3	7.2+/-0.5 [15]		7.71 [106] 7.25(constrained) [19]	6.45 +/- 0.5 [15] 6.2 +/- 0.1 [115]	7.9 +/- 0.2 [19] 7.07 [106] 6.2 +/- 0.1 [115]

Obviously resulting from the distribution adopted in the simulations we note that in the more compact groups taking place for the N configuration (aggregation of trimers) the foreign cations are less connected with the oxygen ions as evidenced by the lower CN(Gd-O). Consequently, those groups encompass more oxygen vacancies and then resemble more to the C-type Gd_2O_3 structure. Thus, following the preceding discussion the percolation threshold of the C-type based structure could arise below x=0.2. Even if they do not explicitly mention a percolation threshold for the x=0.2 value Presto *et al.* [121] recently consider this value as a key parameter in the evolution of the structure and conductivity in Sm-doped ceria. The percolation threshold concept cannot on itself explains the structure change and the evolution of the ionic conductivity of the doped ceria but the whole percolation theory

seems to be a powerful mean to participate to the debate if other ideas could also be taken in consideration as the effective medium theory, the fractal dimension, the tortuosity and the random walk theory. The percolation theory is largely evocated for composite materials (conductor/insulator) [118] where an abrupt rise in dc conductivity is observed around a threshold value up to a maximum. For the doped fluorite materials, a bell shape curve is noted as it is also the case for dispersed ionic conductors in insulating matrix and for some glassy ionic conductors where the percolation concept has been successfully used to described the evolution of the ionic conductivity [122].

We have evidenced in this study that the defect arrangement inside the fluorite lattice leads to large structural changes (lattice parameter, bond length, coordination number, RE site percolation threshold). It is then important to note that the calculation of the total energy E for all the composition and for the two configurations always leads to a higher stability for the N configuration as it can be seen in Fig. 11 where the averaged difference $(E_R-E_N)/N_{at}$ is plotted against x with N_{at} the total number of atoms. This result is in accordance with the higher disorder observed for the R configuration.

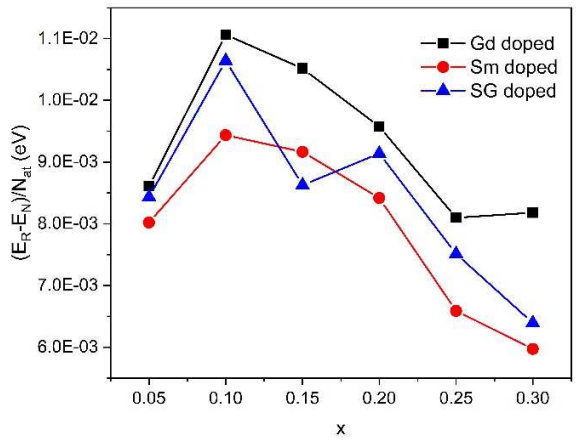

Fig. 11. Evolution of $(E_R-E_N)/N_{at}$ as a function of the composition for the three systems.

With the parameter set chosen in this study the E_R-E_N maximum occurs for a composition where x is in the range [0.1-0.15] and the higher difference is always obtained for the Gd-doped ceria system. Beyond

this range the difference decreases indicating that the two distributions become more and more energetically close.

4. Conclusion

In this work we apply the Molecular Dynamics simulation to study the structural evolution of Gd, Sm-doped and Gd/Sm co-doped ceria with the doping ratio. Inside the starting fluorite structure, the Rare Earth (RE) doping cations and oxygen vacancies are distributed randomly (R) or as randomly distributed trimers (N). The defect arrangement clearly influences the structure of the doping system for a given doping ratio. All the trends denoted here are the same for the Gd-doped and Sm-doped ceria and the co-doped system mainly behaves as an average or a superposition of the parent single doped systems. The lattice parameters extracted from the literature lie between the R and N lattice parameters calculated here whatever the doping lattice letting suppose a great diversity of the defect arrangements in the synthesised samples. The chemical expansion as the oxygen vacancy radius (r_v) depend on the doping cation and the defect distribution with the average value of r_v close to the one found in the literature [66, 96] for the host CeO_2. The calculation of the Radial Distribution Functions (RDF) allows to observe two components for the Ce-Ce, Ce-RE and RE-RE (RE= Gd, Sm, Gd/Sm) bond length as it is the case in the C-type RE_2O_3 structure with a weight of those two components linked to the defect distribution. For all the ionic pairs the RDF first peak is fitted by a log-normal distribution where asymmetry is accounted. The FWHM and asymmetry parameter for the M-O bond then reflect the disorder and the possible creation of a second bond length population. Those parameters decrease in the sequence RE-O (Random), RE-O (Neighbour), Ce-O (Random), Ce-O (Neighbour) indicating a higher disorder in the R configuration than in the N one. When the O-O pair correlation function is extended up to 5 Å a fourth peak appears in the case of the doped ceria which is thus a signature of the presence of the defects. The

RE site percolation threshold for the R configuration is around x=0.2 in accordance with the theoretical value for a FCC lattice. For the N configuration we note that this threshold is lower than x=0.2, ~~for the N distribution~~ we also note that the M-M groups are ~~with~~ more compact ~~groups~~ and encompass ~~and~~ more oxygen vacancies than in the case of the R configuration. We can thus suppose a structure of those groups closer to the C-type RE_2O_3 one for the N configuration than for the R configuration. ~~as expected by the design of our simulations.~~

References

[1] H. Inaba, H. Tagawa, Ceria-based solid electrolytes, Solid State Ion. 83 (1996) 1-16.

[2] J.A. Kilner, Fast oxygen transport in acceptor doped oxides, Solid State Ion. 129 (2000) 13-23.

[3] M. Coduri, S. Checchia, M. Longhi, D. Ceresoli, M. Scavini, Rare earth doped ceria: the complex connection between structure and properties, Front. Chem. 6 (2018) 526.

[4] D.J.L. Brett, A. Atkinson, N.P. Brandon, S.J. Skinner, Intermediate temperature solid oxide fuel cell, Chem. Soc. Rev. 37 (2008) 1568-1578.

[5] S. Zha, C. Xia, G. Meng, Effect of Gd (Sm) doping on properties of ceria electrolyte for solid oxide fuell cells, J. Power Sources 115 (2003) 44-48.

[6] Y. Guo, M. Bessaa, S. Aguado, M.C. Steil, D. Rembelski, M. Rieu, J.P Viricelle, N. Benameur, C. Guizard, C. Tardivat, P. Vernoux, D. Farrusseng, An all porous solid oxide fuel cell (SOFC): a bridging technology between dual and single chamber SOFCs, Energy Environ. Sci. 6 (2013) 2119-2123.

[7] C. Shao, A. Shen, M. Zhang, X. Meng, C. Song, Y. Liu, X. Gao, P. Wang, W.Bu, Oxygen vacancies-enhanced CeO_2:Gd nanoparticles for sensing tumor vascular microenvironment by magnetic resonance imaging, ACS Nano 12 (2018) 12629-12637.

[8] A. Rangaswamy, P. Sudarsanam, B. M. Reddy, Rare earth metal doped CeO_2-based catalytic materials for diesel soot oxidation at lower temperatures, J. Rare Earths 33 (2015) 1162-1169.

[9] R. Korobko, A. Patlolla, A. Kossoy, E. Wachtel, H. L. Tuller, A. I. Frenkel, I. Lubomirsky, Giant electrostriction in Gd-doped ceria, Adv. Mater. 24 (2012) 5857-5861.

[10] J.A. Kilner, Defects and conductivity in ceria-based oxides, Chem. Lett. 37 (2008) 1012-1015.

[11] R. Schmitt, A Nenning, O. Kraynis, R. Korobko, A. I. Frenkel, Igor, Lubomirsky, S. M. Haile, J.L.M. Rupp, A review of defect structure and chemistry in ceria and its solid solutions. Chem. Soc. Rev. 49 (2020) 554-592.

[12] J.A. Purton, A. Archer, N. L. Allan, D.S.D. Gunn, Growth of nano-domains in Gd-CeO2 mixtures: hybrid Monte Carlo simulations, J. Mater. Chem. A 4 (2016) 4592-4602

[13] S. Grieshammer, B.O.H. Grope, J. Koettgen, M. Martin, A combined DFT+U and Monte Carlo study on rare earth doped ceria, Phys. Chem. Chem. Phys. 16 (2014) 9974-9986.

[14] T. Ohashi, S. Yamazaki, T. Tokunaga, Y. Arita, T. Matsui, T. Harami, K. Kobayashi, EXAFS study of $Ce_{1-x}Gd_xO_{2-x/2}$, Solid State Ion. 113-115 (1998) 559-564.

[15] H. Deguchi, H. Yoshida, T. Inagaki, M. Horiuchi, EXAFS study of doped ceria using multiple data set fit, Solid State Ion. 176 (2005) 1817-1825.

[16] S. C. Shirbhate, A. K. Yadav, S. A. Acharya, Extended x-ray absorption fine structure spectroscopy and x-ray absorption near edge spectroscopy study of aliovalent doped ceria to correlate local structural changes with oxygen vacancies clustering, Appl. Phys. Lett. 108 (2016) 143501.

[17] T. Taniguchi, T. Watanabe, N. Sugiyama, A. K. Subramani, H. Wagata, N. Matsushita, M.Yoshimura, Identifying defects in ceria-based nanocrystals by UV resonance Raman spectroscopy, J. Phys. Chem. *C* 113 (2009) 19789–19793.

[18] H. Yamamura, S. Takeda, K. Kakinuma, Relationship between oxide-ion conductivity and dielectric relaxation in Sm-doped CeO_2, Solid State Ion. 178 (2007) 889-893.

[19] F. Giannici, G. Gregori, C. Aliotta, A. Longo, J. Maier, A. Martorana, Structure and oxide ion conductivity: local order, defect interactions and grain boundary effects in acceptor-doped ceria, Chem. Mater. 26 (2014) 5994-6006.

[20] J. Koettgen, M. Martin, Coordination numbers in Sm-doped ceria using X-ray absorption spectroscopy, J. Phys. Chem. C 123 (2019) 6333–6339.

[21] C. Artini, G. A. Costa, M. Pani, A Lausi, J. Plaisier, Structural characterization of the CeO_2/Gd_2O_3 mixed system by synchrotron X-ray diffraction, J. Solid State Chem. 190 (2012) 24-28.

[22] W. Chen, A. Navrotsky, Thermochemical study of trivalent-doped ceria systems: CeO_2-$MO_{1.5}$ (M=La, Gd, and Y), J. Mater. Res. 21 (2006) 3242-3251.

[23] V. Butler, C.R.A Catlow, B.E.F. Fender, J.H. Harding, Dopant ion radius and ionic conductivity in cerium dioxide, Solid State Ion. 8 (1983) 109-113.

[24] X. Wei, W. Pan, L. Cheng, B.Li, Atomistic calculation of association energy in doped ceria, Solid State Ion. 180 (2009) 13-17.

[25] S. Vives, C. Meunier, Defect cluster arrangements and oxygen vacancy migration in Gd doped ceria for different interatomic potentials, Solid State Ion. 283 (2015)137-144.

[26] Z.P. Li, T. Mori, F. Ye, D. Ou, J. Zou, J. Drennan, Ordered structures of defect clusters in gadolinium-doped ceria, J. Chem. Phys. 134 (2011) 224708.

[27] B. Wang, R. J. Lewis, A. N. Cormack, Computer simulations of large-scale defect clustering and nanodomain structure in gadolinia-doped ceria, Acta Mater. 59 (2011) 2035-2045.

[28] F. Ye, T. Mori, D. R. Ou, A. N. Cormack, R. J. Lewis, J. Drennan, Simulation of ordering in large defect clusters in gadolinium-doped ceria, Solid State Ion. 179 (2008) 1962-1967.

[29] M. Asher, O. Dieguez, A computational study of gadolinium-doped ceria: relationship between atomic arrangement and electrostriction, *APL Mater.* 7 (2019) 041109.

[30] P.P. Dholabhai, J. B. Adams, P. Crozier, R. Sharma, A density functional study of defect migration in gadolinium doped ceria, Phys. Chem. Chem. Phys. 12 (2010) 7904-7910.

[31] Z. Fu, Q. Sun, D. Ma, N. Zhang, Y. An, Z. Yang, Effect of Sm doping content on the ionic conduction of CeO_2, in SOFCs from first principles, Appl. Phys. Lett. 111 (2017) 023903.

[32] N. Nakayama, M. Martin, First-principles study on defect chemistry and migration of oxide ions in ceria doped with rare-earth cations, Phys. Chem. Chem. Phys. 11 (2009) 3241-3249.

[33] H. Yoshida, T. Inagaki, K. Miura, M. Inaba, Z. Ogumi, Density functional theory calculation on the effect of local structure of doped ceria on ionic conductivity, Solid State Ion. 160 (2003) 109-116.

[34] H. Wang, A. Chroneos, U. Schwingenschlogl, Impact of doping on the ionic conductivity of ceria: A comprehensive model, J. Chem. Phys. 138 (2013) 224705.

[35] A.K. Lucid, P.R.L. Keating, J.P. Allen, G.W. Watson, Structure and Reducibility of CeO_2 doped with trivalent cations, J. Phys. Chem C 120 (2016) 23430-23440.

[36] Y. Tang, H. Zuang, L. Cui, C. Ouyang, S. Shi, W. Tang, H. Li, J.S. Lee, L. Chen, First-principles investigation on redox properties of M-doped CeO_2 (M= Mn, Pr, Sn, Zr), Phys. Rev. B 82 (2010) 125104.

[37] S. Grieshammer, M. Martin, Influence of defect interactions on the free energy of reduction in pure and doped ceria, J. Mat. Chem. A 5 (2017) 9241-9249.

[38] H. Inaba, R. Sagawa, H. Hayashi, K. Kawamura, Molecular dynamics simulation of gadolinia-doped ceria, Solid State Ion. 122 (1999) 95-103.

[39] Z. Cui, Y. Sun, Y. Chen, J. Qu, Semi-ab initio interionic potential for gadolinia-doped ceria, Solid State Ion. 187 (2011) 8-18.

[40] A. Tarancon, A. Morata, F. Peiro, G. Dezanneau, A molecular dynamics study on the oxygen diffusion in doped fluorites: The effect of the dopant distribution, Fuel Cells 11 (2011) 26-37.

[41] H. Hayashi, R. Sagawa, H. Inaba, K. Kawamura, Molecular dynamics calculations on ceria-based solid electrolytes with different radius dopants, Solid State Ion. 131 (2000) 281-290.

[42] C.W. Huang, W.C.J. Wei, C.S. Chen, J.C. Chen, Molecular dynamics simulation on ionic conduction process of oxygen in $Ce_{1-x}M_xO_{2-x/2}$, J. Eur. Ceram. Soc. 31 (2011) 3159-3169.

[43] P.P. Dholabhai, S. Anwar, J. B. Adams, P. Crozier, R. Sharma, Kinetic lattice Monte Carlo model for oxygen vacancy diffusion in praseodymium doped ceria: Applications to materials design, J. Solid State Chem. 184 (2011) 811-817.

[44] B.O.H. Grope, T. Zacherle, N. Nakayama, M. Martin, Oxygen ion conductivity of doped ceria: A kinetic Monte Carlo study, Solid State Ion. 225 (2012) 476-183.

[45] A. Oaks, D. Yun, B. Ye, W.Y. Chen, J. Stubbins, Kinetic Monte Carlo model of defect transport and irradiation effects in La-doped CeO_2, J. Nucl. Mater. 414 (2011) 145-149.

[46] D.S.D. Gunn, N. L. Allan, J. A. Purton, Adaptive kinetic Monte Carlo simulation of solid oxide fuel cell components, J. Mater. Chem. A 2 (2014) 13407-13414.

[47] D. Van Laethem, J. Deconinck, A. Hubin, Ionic conductivity of space charge layers in acceptor doped ceria, J. Eur. Ceram. Soc. 39 (2019) 432-441.

[48] P.A. Žguns, A.V. Ruban, N.V. Skorodumova, Ordering and phase separation in Gd-doped ceria: a combined DFT, cluster expansion and Monte Carlo study, Phys. Chem. Chem. Phys. 19 (2017) 26606-26620.

[49] P.A. Žguns, A.V. Ruban, N.V. Skorodumova, Phase diagram and oxygen-vacancy ordering in the CeO_2-Gd_2O_3 system: a theoretical study, Phys. Chem. Chem. Phys. 20 (2018) 11805-11818.

[50] C. Guizard, A. Julbe, O. Robbe, S. Sarrade, Synthesis and oxygen transport characteristics of dense and porous cerium/gadolinium oxide materials: interest in membrane reactors, Catal. Today 104 (2005) 120-125.

[51] O. Kraynis, J. Timoshenko, J. Huang, H. Singh, E. Wachtel, A.I. Frenkel, I. Lubomirsky, Modeling strain distribution at the atomic level in doped ceria films with extended X-ray absorption fine structure spectroscopy, Inorg. Chem. 58 (2019) 7527-7536.

[52] H. Yahiro, K. Eguchi, H. Arai, Electrical properties and reducibilities of ceria-rare earth oxide and their application to solid oxide fuel cell, Solid State Ion. 36 (1989) 71–75.

[53] A. Arabaci, Effect of Sm and Gd dopants on structural characteristics and ionic conductivity of ceria, Ceram. Int. 41 (2015) 5386–5842.

[54] G.B. Balazs, R.S. Glass, Ac impedance studies of rare earth oxide doped ceria, Solid State Ion. 76 (1995) 155–162.

[55] K. Eguchi, T. Setoguchi, T. Inoue, H. Arai, Electrical properties of ceria-based oxides and their application to solid oxide fuel cells, Solid State Ion. 52 (1992) 165–172.

[56] A.J. Jacobson, Materials for solid oxide fuel cells, Chem. Mater. 22 (2010) 660–674.

[57] L.B. Winck, J.L. de Almeida Ferreira, J.M.G. Martinez, J.A. Araujo, A.C.M. Rodrigues, C.R.M. da Silva, Synthesis, sintering and characterization of ceria-based solid electrolytes codoped with samaria and gadolinium using the Pechini method, Ceram. Int. 43 (2017) 16408-16415.

[58] A.V. Coles-Aldridge, R.T. Baker, Ionic conductivity in multiply substituted ceria based electrolytes, Solid State Ion. 316 (2018) 9-19.

[59] F.Y. Wang, B-Z. Wan, S. Cheng, Study on Gd^{3+} and Sm^{3+} co-doped ceria based electrolytes, J. Solid State Electr. 9 (2005) 168-173.

[60] H. Yoshida, H. Deguchi, K. Miura, M. Horiuchi, T.Inagaki, Investigation of the relationship between the ionic conductivity and the local structures of singly and doubly doped ceria compounds using EXAFS measurement, Solid State Ion. 140 (2001) 191-199.

[61]: K. M. Kasse, J. C. Nino, Ionic conductivity of $Sm_xNd_yCe_{0.9}O_{2-\delta}$ codoped ceria electrolytes, J. Alloys Compd. 575 (2013) 399-402.

[62] H. Wang, A. Chroneos, C. Jiang, U. Schwingenschlogl, Special quasirandom structures for gadolinia-doped ceria and related materials, Phys. Chem. Chem. Phys. 14 (2012) 11737-11742.

[63] D. R. Ou, F. Ye, T. Mori, Defect clustering and local ordering in rare earth co-doped ceria, Phys. Chem. Chem. Phys. 13 (2011) 9554-9560.

[64] M.J.D. Rushton, A. Chroneos, S.J. Skinner, R.W. Grimes, Effect of strain on the oxygen diffusion in yttria and gadolinia co-doped ceria, Solid State Ion. 230 (2013) 37-42.

[65] M. Burbano, S. Nadin, D. Marrocchelli, M. Salanne, G.W. Watson, Ceria co-doping: synergetic or average effect? Phys. Chem. Chem. Phys. 16 (2014) 8320-8331.

[66]: S. Plimpton, Fast Parallel Algorithms for Short-Range Molecular Dynamics, J. Comp. Phys. 117 (1995) 1-19.

[67]: P. Hirel, Atomsk: A tool for manipulating and converting atomic data files, Comput. Phys. Comm. 197 (2015) 212-219.

[68]: S. Vives, D. Ramel, C. Meunier, Molecular Dynamics Study in the $Ce_{0.9}M_{0.1}O_{1.95}$ (M=Gd, Sm) doped and co-doped CeO_2 Systems: Structure and Oxygen Diffusion, Ceram. Int. 45 (2019) 21625-21634.

[69]: M. Wojdyr, *Fityk*: a general-purpose peak fitting program, J. Appl. Cryst. 43 (2010) 1126-1128.

[70] R. D. Shannon, C.T Prewitt, Effective ionic radii in oxides and fluorides, Acta Cryst. B 25 (1969) 925-946.

[71] R. D. Shannon, Revised effective radii and systematic studies of interatomic distances in halides and chalcogenides, Acta Cryst. A 32 (1976) 751-767.

[72] D. J. Kim, Lattice parameters, ionic conductivities, and solubility limits in fluorite-structure MO_2 oxide (M= Hf^{4+}, Zr^{4+}, Ce^{4+}, Th^{4+}, $U4^{+}$) solid solution, J. Am. Ceram. Soc. 72 (1989) 1415-1421.

[73] S. J. Hong, A. Virkar, Lattice parameters and densities of rare-earth oxide doped ceria electrolyte, J. Am. Ceram. Soc. 78 (1995) 433-439.

[74] A. Nakamura, New defect-crystal-chemical approach to non-Vegardianity and complex defect structure of fluorite-based MO_2-$LnO_{1.5}$ solid solutions (M^{4+}=Ce, Th; Ln^{3+}=lanthanide) part I: Model description and lattice parameter data analysis, Solid State Ion. 181 (2010) 1543-1564.

[75] A. Kossoy, Q. Wang, R. Korobko, V. Grover, Y. Feldman, E. Wachtel, A. K. Tyagi, A. I. Frenkel, L. Lubomirsky, Evolution of the local structure at the phase transition CeO_2-Gd_2O_3 solid solution, Phys. Rev. B 87 (2013) 054101.

[76] A. Nakamura, K. Imai, N. Igawa, Y. Okamoto, E. Yamamoto, S. Matsukawa, M. Takahashi, ^{155} Gd Mössbauer spectroscopic and powder X-ray diffraction study of CeO_2-$GdO_{1.5}$ solid solution, Hyperfine Interact. 207 (2012) 67-71.

[77] M. Scavini, M. Coduri, M. Allieta, M. Brunelli, C. Ferrero, Probing Complex Disorder in $Ce_{1-x}Gd_xO_{2-x/2}$ Using the Pair Distribution Function Analysis, Chem. Mater. 24 (2012) 1338-1345.

[78] M. Yashima, T. Takizawa, Atomic displacement parameters of ceria doped with rare-earth oxide $Ce_{0.8}R_{0.2}O_{1.9}$ (R=La, Nd, Sm Gd, Y and Yb) and correlation with oxide-ion conductivity, J. Phys. Chem. C 114 (2010) 2385-2392.

[79] J. Zhang, C. Ke, H. Wu, J. Yu, J. Wang, Y. Wang, Solubility limits, crystal structure and lattice thermal expansion of Ln_2O_3 (Ln= Sm, Eu, Gd) doped CeO_2, J. Alloys Compd. 718 (2017) 85-91.

[80] K. Huang, M. Feng, J.B. Goodenough, Synthesis and electrical properties of dense $Ce_{0.9}Gd_{0.1}O_{1.95}$ Ceramics, J. Am. Ceram. Soc. 81 (1998) 357-362.

[81] V.V. Kharton, F.M. Figueiredo, L.Navarro, E.N. Naumovich, A.V. Kovalevsky, A.A. Yaremchenko, A.P. Viskup, A. Carneiro, F.M.B. Marques, J.R. Frade, Ceria-based materials for solid oxide fuel cells, J. Mater. Sci. 36 (2001) 1105-1117.

[82] S. Omar, E.D. Wachsman, J.L. Jones, J.C. Nino, Crystal structure-ionic conductivity relationships in doped ceria systems, J. Am. Ceram. Soc. 92 (2009) 2674-2681.

[83] I. Riess, D. Braunshtein, D.S. Tannhauser, Density and ionic conductivity of sintered $(CeO_2)_{0.82}(GdO_{1.5})_{0.18}$, J. Am. Ceram. Soc. 64 (1981) 479-485.

[84] Z. Tianshu, P. Hing, H. Huang, J. Kilner, Ionic conductivity in the CeO_2-Gd_2O_3 system ($0.05 \leq Gd/Ce \leq 0.4$) prepared by oxalate coprecipitation, Solid State Ion. 148 (2002) 567-573.

[85] V. Grover, A.K. Tyagi, Phase relations, lattice thermal expansion in CeO_2-Gd_2O_3 system, and stabilization of cubic gadolinia, Mater. Res. Bull. 39 (2004) 859-866.

[86]: T. Mahata, G. Das, R.K. Mishra, B.P. Sharma, Combustion synthesis of gadolinia doped ceria powder, J. Alloys Compd. 391 (2005) 129-135.

[87] U. Hennings, R. Reimert, Investigation of the structure and the redox behavior of gadolinium doped ceria to select a suitable composition for use as catalyst support in the steam reforming of natural gas, Appl. Catal. A-Gen. 325 (2007) 41-49.

[88]: E. Yu. Pikalova, A.A. Murashkina, V.I. Maragou, A.K. Demin, V.N. Strekalovsky, P.E. Tsiakaras, CeO_2 based materials doped with lanthanides for applications in intermediate temperature electrochemical devices, Int. J. Hydrogen. Energy 36 (2011) 6175-6183.

[89] M.Coduri, M. Scavini, M. Pani, M.M. Carnasciali, H. Klein, C. Artini, From nano to microcrystals : effect of different synthetic pathways on defects architecture in heavily Gd-doped ceria, Phys. Chem. Chem. Phys. 19 (2017) 11612-11630.

[90] S. C. Shirbhate, A. K. Yadav, S. A. Acharya, A.P.Sagdeo, S.N. Jha, Local structural study of doped-ceria by EXAFS spectroscopy, AIP Conference Proceedings 1731 (2016) 040003.

[91] M. Dudek, M. Mroz, L. Zych, E. Drozdz-Ciesla, Synthesis of ceria-based nanopowders suitable for manufacturing solid electrolytes, Materials Sci-Poland 26 (2008) 319-329.

[92] W. Zajac, J. Molanda, Electrical conductivity of doubly doped ceria, Solid State Ion. 179 (2008) 154-158.

[93] A.V. Coles-Aldridge, R.T. Baker, Oxygen ion conductivity in ceria-based electrolytes co-doped with samarium and gadolinium, Solid State Ion. 347 (2020) 115255.

[94] C. Artini, M. Pani, M.M. Carnasciali, M.T. Buscaglia, J.R. Plaisier, G.A. Costa, Structural features of Sm- and Gd-doped ceria studied by synchrotron X-ray diffraction and μ-Raman spectroscopy, Inorg. Chem. 54 (2015) 4126-4137.

[95] M. Coduri, P. Massala, M. Allieta, I. Peral, M.Brunelli, C. A. Biffi, M. Scavini, Phase transformations in the CeO_2-Sm_2O_3 system: a multiscale powder diffraction investigation, Inorg. Chem. 572 (2018) 879-891.

[96] S. Soni, S. Kumar, B. Dalela, S. Kumar, P.A. Alvi, S. Dalela, Defects and oxygen vacancies tailored structural and optical properties in CeO_2 nanoparticles doped with Sm^{3+} cations, J. Alloys Compd. 752 (2018) 520-231.

[97] S.F. Wang, C.T. Yeh, Y.R. Wang, Y.C. Wu, Characterization of samarium-doped ceria powders prepared by hydrothermal synthesis for use in solid state oxide fuel cells, J. Mater. Res. Technol. 2 (2013) 141-148.

[98] Y.P Fu, S.B. Wen, C.H. Lu, Preparation and characterization of samaria-doped ceria electrolyte materials for solid oxide fuel cells, J. Am. Ceram. Soc. 91 (2008) 127-131.

[99] T. Hisashige, Y. Yamamura, T. Tsuji, Thermal expansion and Debye temperature of rare earth-doped ceria, J. Alloys Compd. 408-412 (2006) 1153-1156.

[100] M.R. Kosinski, R. T. Baker, Preparation and property-performance relationships in samarium-doped ceria nanopowders for solid oxide fuel cell electrolytes, J. Power Sources 196 (2011) 2498-2512.

[101] H. Yahiro, Y. Eguchi, K. Eguchi, H. Arai, Oxygen ion conductivity of ceria-samarium oxide system with fluorite structure, J. Appl. Electrochem. 18 (1988) 527-531.

[102] A. Kossoy, Y. Feldman, R. Korobko, E. Wachtel, I. Lubomirsky, J. Maier, Influence of point-defect reaction kinetics on the lattice parameter of $Ce_{0.8}Gd_{0.2}O_{1.9}$, Adv. Funct. Mater. 19 (2009) 634-641.

[103] D. Marrocchelli, S. R. Bishop, H. L. Tuller, B. Yildiz, Understanding chemical expansion in non-stoichiometric oxides: ceria and zirconia case studies, Adv. Funct. Mater. 22 (2012) 1958-1965.

[104] C. Chatzichristodoulou, P. Norby, P.V. Hendriksen, M.B. Mogensen, Size of oxide vacancies in fluorite and perovskite structured oxides, J. Electroceram. 34 (2015) 100-107.

[105] C. Artini, Rare-earth-doped ceria systems and their performance as solid electrolytes: a puzzling tangle of structural issues at the average and local state, Inorg Chem. 57 (2018) 13047-13062.

[106] H. Nitani, T. Nakagawa, M. Yamanouchi, T. Osuki, M. Yuya, T.A. Yamamoto, XAFS and XRD study of ceria doped with Pr, Nd and Sm, Mat. Lett. 58 (2004) 2076.

[107] Y. Yamazaki, T. Matsui, T. Ohashi, Y. Arita, Defect structures in doped CeO_2 studied by using XAFS spectrometry, Solid State Ion. 136-137 (2000) 913-920.

[108] M. Coduri, M. Scavini, M. Allieta, B. Brunelli, C. Ferrero, Local disorder in yttrium doped ceria ($Ce_{1-x}Y_xO_{2-x/2}$ probed by joint x-ray and neutron powder diffraction, J. Phys.: Conf. Ser. 340 (2012) 012056.

[109] A. Stukowski, Visualization and analysis of atomistic simulation data with OVITO-the open visualization tool, Modelling Simul. Mater. Sci. Eng. 18 (2010) 015012.

[110] K. Momma, F. Izumi, VESTA 3 for three-dimensional visualization of crystal, volumetric and morphology data, J. Appl. Cryst. 44 (2011) 1272-1276.

[111] M. Scavini, M. Coduri, M. Allieta, P.Masala, S.Cappelli, C. Oliva, M. Brunelli, F. Orsini, C. Ferrero, Percolating hierarchical defect structures drive phase transformation in $Ce_{1-x}Gd_xO_{2-x/2}$: a total scattering study, IUCrJ 2 (2015) 511-522.

[112] M. Sahimi, Applications of percolation theory, 1994, CRC Press.

[113] M. Meyer, N. Nicoloso, V. Jaenisch, Percolation model for anomalous conductivity of fluorite-related oxides, Phys. Rev. B 56 (1997) 5961-5966.

[114] R. Zallen, The physics of amorphous solids, chapter IV, WILEY-VCH Verlag GmbH & Co. KGaA, Weinheim 2004.

[115] C. Artini, M. M. Carnasciali, J. R. Plaisier, G. A. Costa, M. Pani, A novel method for the evaluation of Rare Earth (RE) coordination number in RE-doped ceria through Raman spectroscopy, Solid State Ion. 311 (2017) 90-97.

[116] S. C. Shirbhate, K. Singh, S. A. Acharya, A. K. Yadav, Review on local structural properties of ceria based electrolytes for IT-SOFC, Ionics 23 (2017) 1049-1057.

[117] S. Kirkpatrick, Percolation and conduction, Rev. Mod. Phys. 45 (1973) 574-588.

[118]118 D.S. McLachlan, M. Blaszkiewicz, R.E. Newnham, Electrical resistivity of composite, J. Am. Ceram. Soc. 73 (1990) 2187-2203.

[119] P. Li, I. W. Chen, J. E. Penner-Hahn, T. Y. Tien, X-ray absorption studies of ceria with trivalent dopants, J. Am. Ceram. Soc. 74 (1991) 958-967.

[120] R. Korobko, A. Lerner, Y. Li, E. Wachtel, A. I. Frenkel, I. Lubomirski, In-situ extended X-ray absorption fine structure study of electrostriction in Gd doped ceria, App. Phys. Lett. 106 (2015) 042904.

[121] S Presto, C.Artini, M. Pani, M.M. Carnasciali, S. Massardo, M. Viviani, Ionic conductivity and local structural features in $Ce_{1-x}Sm_xO_{2-x/2}$, Phys. Chem. Chem. Phys. 20 (2018) 28338-28345.

[122] A. Bunde, Application of percolation theory in composites and glasses, Solid State Ion. 75 (1995) 147-155.